Large-scale Controls on Atlantic Tropical Cyclone Activity on Seasonal Time Scales

Young-Kwon Lim[1,2], Siegfried D. Schubert[1],
Oreste Reale[1,3], Andrea M. Molod[1,4], Max J. Suarez[1,3] Benjamin M. Auer[1,5]

Corresponding author: Young-Kwon Lim (Young-Kwon.Lim@nasa.gov)

[1]Bldg. 33, code 610.1, 8800 Greenbelt Rd.,
Global Modeling and Assimilation Office, NASA/GSFC, Greenbelt, Maryland, 20771
[2]Goddard Earth Sciences Technology and Research, I. M. Systems Group
[3]Goddard Earth Sciences Technology and Research, Universities Space Research Association (USRA)
[4]Earth System Science Interdisciplinary Center,
University of Maryland, College Park, Maryland
[5]Science Systems and Applications Inc. (SSAI)

May 11, 2016
Submitted to Journal of Climate (Revised version)

Abstract

Interannual variations in seasonal tropical cyclone (TC) activity (e.g., genesis frequency and location, track pattern, and landfall) over the Atlantic are explored by employing observationally-constrained simulations with the NASA Goddard Earth Observing System version (GEOS-5) atmospheric general circulation model. The climate modes investigated are El Niño-Southern Oscillation (ENSO), the North Atlantic Oscillation (NAO), and the Atlantic Meridional Mode (AMM).

The results show that the NAO and AMM can strongly modify and even oppose the well-known ENSO impacts, like in 2005, when a strong positive AMM (associated with warm SSTs and a negative SLP anomaly over the western tropical Atlantic), led to a very active TC season with enhanced TC genesis over the Caribbean Sea and a number of landfalls over North America, under a neutral ENSO condition. On the other end, the weak TC activity during 2013 (characterized by weak negative Niño index) appears caused by a NAO-induced positive SLP anomaly with enhanced vertical wind shear over the tropical North Atlantic. During 2010, the combined impact of the three modes produced positive SST anomalies across the entire low-latitudinal Atlantic and a weaker subtropical high, leading to more early recurvers and thus fewer landfalls despite enhanced TC genesis. The study provides evidence that TC number and track are very sensitive to the relative phases and intensities of these three modes, and not just to ENSO alone. Examination of seasonal predictability reveals that predictive skill of the three modes is limited over tropics to sub-tropics, with the AMM having the highest predictability over the North Atlantic, followed by ENSO and NAO.

1. Introduction

Seasonal tropical cyclone (TC) activity (e.g., genesis frequency and location, track patterns, landfall, life cycle, etc.) over the North Atlantic is characterized by considerable year-to-year variability. A number of atmospheric general circulation models (AGCMs) and statistical models have demonstrated some ability to reproduce interannual variations in TC (hurricane, tropical storm, and tropical depression) frequency over the past few decades (Klotzbach and Gray 2004; LaRow et al. 2008; Zhao et al. 2009; Kim and Webster 2010; Putman and Suarez 2011; Chen and Lin 2013; Bacmeister et al. 2014; Vecchi et al. 2014; Murakami et al. 2015; Wang et al. 2015). The latest NASA "Nature Run", produced by the Global Modeling and Assimilation Office (GMAO) and documented in Gelaro et al. (2015), is particularly remarkable for its high resolution (~7km). It has produced differences in TC activity between 2005 and 2006, which were consistent with observations over each ocean basin including some "difficult" basin such as the northern Indian Ocean, where generally global models perform less than optimally partly due to shorter lifespan and more erratic TC tracks, compared to the Atlantic and Pacific (e.g., Reale et al. 2009).

However, operational forecasting agencies do not issue sub-seasonal and seasonal predictions of the societally most important aspects such as track and landfall distribution (http://www.cpc.noaa.gov/products/outlooks/hurricane-archive.shtml). An active TC season in which most storms are "early recurvers" (i.e., Cape Verde TCs that recurve northeastward at about 45°W instead of crossing the Atlantic) may have less societal impact than an inactive season with a single strike over a highly populated area (e.g, Blake and Gibney 2011). The 2010 TC season is one of those cases in point. The primary factors (e.g., sea surface temperature (SST) and El Niño Southern Oscillation (ENSO)) assumed to control TC activity suggested an active

71 TC genesis (http://www.cpc.noaa.gov/products/outlooks/hurricane2010/May/hurricane.shtml).
72 However, no hurricanes made landfall over the United States (US) (Bell et al. 2011; Wang et al.
73 2011)- in spite of the large number of observed TCs.

74 It has been accepted for more than 50 years that the sign of SLP anomalies over the tropical
75 Atlantic (TA, defined as in Knaff 1997) is correlated with TC activity (Knaff 1997). However,
76 increasing complexity has been added by several recent studies indicating that TC occurrence is
77 related to climate variability through changes in both circulation and thermodynamic conditions
78 (Kossin and Camargo 2009; Kossin et al. 2010; Patricola et al. 2014) controlled by a synergy
79 between the Atlantic Meridional Mode (AMM) (Chiang and Vimont 2004) and ENSO, which are
80 also found to modulate deep convection throughout the tropics (e.g., Colbert and Soden 2012).
81 Moreover, the Madden Julian Oscillation (MJO) appears to control TCs throughout the tropical
82 Atlantic (Mo 2000; Maloney and Hartmann 2000; Camargo et al. 2009; Klotzbach 2010;
83 Klotzbach and Oliver 2015). In addition, a number of studies (Elsner 2003, Kossin et al. 2010)
84 suggested that the North Atlantic Oscillation (NAO) (Wallace and Gutzler 1981; Barnston and
85 Livezey 1987) affects TCs, with the negative NAO eroding the western flank of the North
86 Atlantic subtropical high and allowing TCs to become recurvers. In apparent contrast, Xie et al.
87 (2005) found that TC landfall number along the US east coast is negatively correlated with the
88 NAO phase. The ENSO phase also seems to affect the probability of landfalling TCs (e.g.,
89 O'Brien et al. 1996; Bove et al. 1998; Larson et al. 2005) as well as the presence of TCs in the
90 Caribbean (Tartaglione et al. 2003). Smith et al. (2007) suggest that ENSO impacts on
91 landfalling frequencies over the US is largest on the East Coast from Georgia to Maine, and less
92 so over Florida and the Gulf Coast.

93 In terms of mechanisms, ENSO and AMM are known to impact shear (e.g., Kossin and

Vimont 2007) with La Niña (El Niño) and positive (negative) AMM driving low (high) shear anomalies (Aiyyer and Thorncroft 2006; Shaman et al. 2009). Smirnov and Vimont (2011) showed that a reduction (enhancement) in vertical wind shear occurs with the positive (negative) SST anomalies over the subtropical North Atlantic during the positive (negative) AMM. Camargo et al. (2007) confirmed that the dynamical role of wind shear is as important as any thermodynamic impacts in El Niño years. Patricola et al. (2014) also found that mid-tropospheric moisture as a thermodynamic impact plays an equally important role compared to vertical wind shear in controlling Atlantic TC activity during the AMM.

Despite the vast number of studies focused on the understanding of the physical processes impacting TC activity, surprisingly poor seasonal predictions (in terms of TC counts) are sometimes released. For example, strong TC activity with 14-20 TCs was forecasted for year 2013 due to above-average SSTs across the tropical Atlantic and no El Niño conditions ahead of TC season (http://www.cpc.noaa.gov/products/outlooks/hurricane2013/May/hurricane.shtml). However, the 2013 TC season was characterized by a strong positive sea level pressure (SLP) anomaly and wind shear, conducive to weak TC activity (Blake 2014) with 14 TCs, most of which were short-lived. The 2006 TC season was predicted to be active (http://www.noaanews.noaa.gov/stories2006/s2634.htm, 13-16 TCs forecasted), which did not turned out to be the case (10 TCs with few landfalls). Some authors have suggested a more important role for dust than dynamical modes (e.g., Lau and Kim 2007). On the other hand, the very active TC season in 2005 (observation: 29 (Fig. 2a), operational forecast: 12-15 TCs (http://www.cpc.noaa.gov/products/outlooks/hurricane2005/May/hurricane.html)) and 2010 (http://www.cpc.noaa.gov/products/outlooks/hurricane2010/May/hurricane.html, observation: 21 (Fig. 4a), forecast: 14-23) was reasonably forecasted. However, those two TC seasons were

117 characterized by very different distributions of TC genesis locations and landfalls, which are not
118 products provided by the current operational forecasting agencies on seasonal time scales.

119 While the possibility exists that many more causes, some unknown, affect TC activity, the
120 main objective of this study is to improve our understanding of how the dynamics of large-scale
121 climate variability associated with 3 well-studied modes (ENSO, the AMM, and the NAO) can
122 impact North Atlantic seasonal TC activity. Moreover, this work aims at assessing the ability to
123 predict these major modes of variability using a state-of-the-art atmospheric general circulation
124 model (AGCM). An observational analysis combined with partially constrained simulations with
125 the National Aeronautics and Space Administration (NASA) Goddard Earth Observing System
126 Model version 5 (GEOS-5) AGCM (Rienecker et al. 2008) is carried out. Specifically, we use a
127 "replay" (see section 2) capability that takes advantage of the Modern-Era Retrospective
128 Analysis for Research and Applications (MERRA) reanalysis (Rienecker et al. 2011) to constrain
129 large-scale aspects of the atmosphere in the GEOS-5 simulations.

130 The paper is organized as follows. The analysis data, GEOS-5 model, and the experimental
131 design are described in Section 2. Section 3.1 presents and compares the TC track statistics
132 produced in each of the model experiments. We then quantify the impact of the dominant climate
133 modes of variability on the Atlantic TC activity for selected recent years and discuss the
134 atmospheric large-scale constraints necessary to control the seasonal TC activity (sections 3.2-
135 3.5). Additionally, we explore if this large-scale constraint can also reproduce the observed
136 relationship between TC genesis frequency and the phase of the Madden-Julian Oscillation (MJO)
137 (section 3.6). In section 3.7, we assess the predictability of the dominant climate modes for the
138 last 9 hurricane seasons (2005-2013) simulated by the GEOS-5 AGCM. A discussion and
139 conclusions are given in Section 4.

2. Data, model and experimental design

2.1 Data and model

The study employs: a) the MERRA data (Rienecker et al. 2011) used at native horizontal resolution of 0.5° latitude×0.6667° longitude; and b) model simulations, making use of the NASA GEOS-5 AGCM (Rienecker et al. 2008; Molod et al. 2012). The investigation is focused over North America and the Atlantic Ocean, covering the Atlantic TC seasons (June through November) from 2005 through 2013. Key variables include SST, SLP, lower (850hPa) and upper (200hPa) level horizontal wind, relative humidity at 700hPa, and upper-level (250hPa) geopotential height. The observed TC best track data (HURDAT2) (see Figs. 2a-5a) are obtained from the National Hurricane Center (Landsea and Franklin, 2013). This hurricane database is a post-storm reanalysis which includes all available observations, including from systems which are not available in real time, and is documented online at: http://www.aoml.noaa.gov/hrd/hurdat/newhurdat-format.pdf.

The NASA GEOS-5 was run with 72 hybrid-sigma vertical layers, extending to 0.01 hPa, and ~0.5° latitude/longitude horizontal resolution. The model uses the finite-volume dynamics of Lin (2004), along with a modified version of the Relaxed Arakawa Schubert (RAS) convection scheme of Moorthi and Suarez (1992). A stochastic Tokioka constraint (Tokioka et al. 1988; Lim et al. 2015) is applied to the convective plumes, leading to improved TC genesis without negatively impacting the mean climate (Reed and Jablonowski 2011; Zhao et al. 2012; Lim et al. 2015). The model employs a prognostic cloud microphysics scheme (Bacmeister et al. 2006) and the catchment land surface model developed by Koster et al. (2000). Further details about the GEOS-5 AGCM can be found in Rienecker et al. (2008) and Molod et al. (2012).

2.2 Model Experiments

One of this study's goals is to quantify the dominant large-scale controls on North Atlantic TC tracks, by reproducing the observed TC track statistics in the GEOS-5 simulations and adopting a replay methodology (Rienecker et al. 2008) to systematically constrain different aspects of the simulations.

The Incremental Analysis Update (IAU) approach developed by Bloom et al. (1996), and implemented in the GEOS-5 Data Assimilation System (DAS) is an essential element of our procedure. The IAU approach allows to insert gradually analysis increments produced during the assimilation cycle in the model and has been generalized so that the model can be "replayed" against an existing analysis (MERRA in this study). The IAU (Fig. 1) reads in an existing analysis field at the analysis time, computes an analysis increment (the difference from the first guess) generally over a 6 hour interval, rewinds 3 hours, and forces the model with a scaled version of the increment over the next 6 hours. The model is then run another 3 hours without the analysis increment forcing to provide the next first guess field, at which point the cycle repeats. The replay process therefore consists of a continuous model run that is forced by analysis increments changing every 6 hours. Since the experiments' goal is the evaluation of the large-scale atmospheric control of TC tracks, the analysis increments are spatially filtered (spectral triangular truncation) to retain only the largest planetary scales. It should be emphasized that this filtering procedure does not directly affect or constrain the TCs. The years selected (2005, 2006, 2010 and 2013) are characterized by very different TC intensities and tracks, thus providing a wide range of variability within a limited sample. Three different sets of experiments are performed for the large-scale constraints, with analysis increments: i) filtered to retain only the

first five total wavenumbers (hereafter R5W); ii) filtered to retain the first eight total wavenumbers (R8W), and iii) unconstrained (unfiltered), as a free running simulation here referred to as "Nature Run" (NR). All simulations are done with prescribed weekly sea surface temperature (SST) forcing (the HadISST of Rayner et al. 2003). Each set of experiments consists of three ensemble members initialized from MERRA atmospheric data on May 1st , 2 nd, and 3rd of each year.

3. Results

3.1 TC tracks

The TC tracks for June through November of each year (computed with the same TC detection and tracking algorithm used by Vitart et al. 2003, Knutson et al. 2007, and LaRow et al. 2008) are shown in Figs. 2-5. TC threshold values for relative vorticity, maximum wind speed, warm core, SLP deepening and minimum duration time (Table 1) are similar to those suggested by Walsh et al. (2007) for a 0.5° horizontal resolution model. A key result is that all three experiments successfully reproduce the interannual variations of TC numbers. For example, the experiments indicate an active season (19-22) in 2005 (Fig. 2), although fewer than the observed 29, and produce from 18 to 21 TCs for the active season of 2010, which is close to the observed 20 TCs (Fig. 4). Similarly, the inactive seasons of 2006 and 2013 are well captured by the experiments (Figs. 3 and 5).

A prominent difference between the active 2005 and 2010 seasons is the relative scarcity of Cape Verde systems (i.e., systems whose genesis occur over the Eastern Atlantic, close to Africa) in 2005 with respect to 2010 (Fig. 4a). The fewer instances of eastern Atlantic TC genesis in 2005 season appear closely linked to the negative SLP anomalies in the central and western

Atlantic (Fig. 2a). The 2005 season was not only characterized by exceptional TC genesis, but also by a number of landfalls over the North American continent (Fig. 2a, Table 2). The spatial pattern of TC tracks in the three experiments suggests sensitivity to the simulated SLP anomaly distribution. In fact, the R8W run produces a TC pattern closest to the observed in terms of landfall (Fig. 2c, 3–4th rows in Table 2) and also the largest negative SLP anomalies centered over the Gulf of Mexico and Caribbean Sea (Figs. 2a,c). In contrast, the NR shows an excessively extended SLP anomaly with more Cape Verde systems (Figs. 2d,g,j) and fewer landfalls over the US compared with the other runs (Fig. 2d, Table 2). The R5W shows an intermediate situation between the two in terms of landfalls over the US (3rd row in Table 2).

The inactive 2006 TC season is also best represented by the R8W (Fig. 3). The observations (Fig. 3a) show only 10 TCs and two landfalls (Table 2) with the remaining TCs being recurvers or tracking well to the east of the US coast. Again, the good representation of TC tracks in R8W finds good correspondence with realistic SLP anomalies (Figs. 3a,c). In contrast, the NR run produces more landfalls (Figs. 3d,g, 5–6th rows in Table 2) than the other two experiments and the observations, while the R5W (Fig. 3b) shows fewer recurvers than observed, and more landfalls than the R8W but fewer than the NR over the US (5th row in Table 2). As noted before, the ability of producing a realistic SLP anomaly seems to be connected with a realistic track distribution.

In spite of 2010 being another active TC season, the TC track pattern differs significantly from 2005. The observations in Fig. 4a clearly show that TC genesis locations are zonally distributed across the subtropical North Atlantic, in good correspondence with zonally elongated negative SLP anomalies. Wang et al. (2011) argued that the negative SLP anomalies in 2010 could be resulting from a strong eastward expansion of the Atlantic warm pool and may inhibit

the westward expansion of the positive SLP anomaly in the eastern Atlantic. This pattern could be a prominent cause for TCs to recurve far away from the US continent, producing fewer landfalls despite active TC genesis often attributed to La Niña conditions. Landfalling TCs are associated either with westward moving TCs crossing the Atlantic toward Central America or with systems generated in the Caribbean. TC tracks generated by the R8W and R5W runs are more realistic than the NR run (Figs. 4b-d), including the number of US landfalls, which are strongly overestimated in the NR (cf. Figs. 4d,g, 7th row in Table 2).

2013 was an inactive TC season, with positive SLP anomalies throughout the North Atlantic (Fig. 5a). All three experiments could reproduce the SLP pattern over the Atlantic (Figs. 5b-d), but the NR generated a larger number of TCs with several tracks through the Caribbean Sea and the Gulf of Mexico, overestimating the landfalls over the southeastern US, (Figs. 5d,g, 9th row in Table 2). On the other hand, R8W and R5W produce a smaller number of landfalls and, most important, a prominent feature of the 2013 season: several Cape Verde systems crossing the Atlantic westward with an almost straight trajectory. This finding seems to agree with Elsner (2003), who suggested that a positive anomaly in the North Atlantic subtropical high associated with the NAO favors relatively straight westward TC tracks with little recurvature. The possible impact of the positive NAO on the TC activity for this year will be examined in the next section.

3.2 Three leading climate modes that impact Atlantic TC activity

A rotated EOF (REOF) technique (Richman 1986) is first employed to investigate the variability of seasonal TC track and landfall patterns in the experiments, with the goal of capturing the leading climate modes that could explain the role of monthly SST in modulating Atlantic TC activity. The three leading SST climate modes are ENSO, the North Atlantic

255 Oscillation (NAO) (Wallace and Gutzler 1981; Barnston and Livezey 1987) and the Atlantic
256 Meridional Mode (AMM) (Vimont and Kossin 2007; Smirnov and Vimont 2011). These
257 findings are in good agreement with Kossin et al. (2010).

258 The eigenvectors (the spatial distributions) together with the corresponding principal
259 component (PC) time series of the three modes are shown in Figure 6. All eigenvectors and PC
260 time series are plotted for the positive phase, together with the traditional index time series of
261 these modes (data from the NOAA Climate Prediction Center (CPC) available at:
262 ftp://ftp.cpc.ncep.noaa.gov/wd52dg/data/indices/tele_index.nh). The PC time series are in good
263 agreement with the phases of the ENSO and AMM indices (Figs. 6d,f), whereas the PCs,
264 correspond with the NAO in 2005, 2006, 2007, 2010, 2012 and 2013, but not in 2008, 2009 and
265 2011 (Fig. 6e). It is possible that since the NAO is primarily an atmospheric mode (Barnston and
266 Livezey 1987) it is marginally affected by SST.

267 The El Niño mode is characterized by positive SST anomalies over the tropical eastern
268 Pacific, positive anomalies over the extratropical Atlantic, and negative anomalies across the
269 tropical Atlantic and the Caribbean (Fig. 6a) (Deser et al. 2010), which contribute to unfavorable
270 conditions for TC genesis, with the opposite pattern during the cold ENSO phase.

271 The NAO-related SST REOF shown in Fig. 6b is characterized by a north-south tripole
272 across the extra-tropical Atlantic. Two zones of negative SST anomalies occur between 20°-
273 30°N and 50°-60°N, separated by a zone of positive anomalies. The tropical Atlantic is
274 characterized by relatively weak negative (positive) SST anomalies during the positive (negative)
275 phase of the NAO, providing unfavorable (favorable) conditions for TC activity. This result
276 appears in agreement with Elsner and Jagger's (2006) statistical assessment of the NAO phase
277 impact on TCs.

It is particularly noteworthy that the positive phase of the AMM mode (Fig. 6c) characterized by positive SST anomalies throughout the tropical Atlantic as far as ~30°N (Chiang and Vimont 2004), can be sufficiently strong to offset the negative SST anomalies over the same region associated with El Niño events (cf. Fig. 6c and 6a). Figure 6f shows that both 2005 and 2010 are characterized by strong positive AMM episodes, while 2006 and 2013 are characterized by near-neutral (or weak positive) AMM conditions.

3.3 Regressed atmospheric anomalies associated with the large-scale leading modes

The next step is to regress the leading modes identified above (ENSO, NAO and AMM) against each PC time series of ENSO, NAO, and AMM for the years 2005-2013, to assess their impact on atmospheric variables such as SLP, z250, vertical wind shear and relative humidity at 700hPa (RH700). For example, the regressed atmospheric anomalies for the ENSO mode at grid point (x,y) is given as

$$R_{ENSO}(x,y) = \sum_{t=1}^{nt} T(x,y,t) \cdot TS_{ENSO}(t), \quad (1)$$

where $T(x,y,t)$ is the anomaly field in question at time step t, and $TS_{ENSO}(t)$ represents the normalized monthly PC time series for ENSO. *nt* is the length of the analysis period. Here *nt* is given as 108 (9 years × 4 months (June-September) × 3 members). Similar calculations are made for the NAO and AMM.

Figure 7 shows the atmospheric fields regressed against ENSO. The observed response to El Niño shows the expected pattern of negative SLP anomalies over the eastern tropical Pacific, and positive SLP anomalies at tropical to subtropical Atlantic, suggestive of unfavorable conditions for TC genesis over the regions (Fig. 7a). This pattern is reproduced in both the R8W and R5W runs (Figs. 7e,i) but not realistically in the NR run (Fig. 7m). The RH700 exhibits negative anomalies associated with El Niño, primarily over the Caribbean Sea and the tropical

western-central Atlantic (Figs. 7b,f,j,n), where the positive SLP anomalies dominate. As for the vertical wind shear, only the R8W run produces realistic vertical wind shear anomalies (Figs. 7c,g,k,o). The climatological vertical wind shear over the Atlantic during the TC season is generally controlled by the tropical easterly jet (TEJ) and by subtropical high-level winds. While the TEJ is confined at latitudes lower than 15°N and is the prominent cause of easterly shear (hatched in Figs. 7c,g,k,o), westerly shear is controlled by either easterly flow decreasing with height, or by upper-level westerly flow which may be associated with the subtropical jet. Thus, the positive wind shear anomaly across the US and the Atlantic at ~30–40°N represents enhanced vertical westerly shear, and appears dynamically linked to an enhanced upper-level westerly subtropical jet during El Niño (Zhu et al. 2012), which opposes the northward progression of TCs.

Figure 8 is the same as Fig.7, but for the NAO mode. The top panel in Fig. 8 shows that the North Atlantic midlatitudes are dominated by positive SLP anomalies during the positive NAO, creating unfavorable conditions for TC genesis and evolution, in agreement with Knaff (1997) and Kossin et al. (2010) who also found that positive (negative) SLP anomalies associated with the positive (negative) phase of the May-June NAO are correlated with a local decrease (increase) in TC genesis. In addition, Xie et al. (2005) argued that the negative NAO favors more landfalling hurricanes over the US southeast region. Our model results indicate that the R8W is again more realistic in reproducing the details (especially the gradients) of the observationally-based regressed SLP pattern (Figs. 8a,e,i,m) with respect to the R5W and the NR.

The observations and R8W suggest that the positive phase of the NAO is associated with positive RH700 anomalies over the western subtropical Atlantic, to the southwest of the positive SLP anomaly in mid-latitudes Atlantic (Figs. 8b,f) and with an area of negative RH700

anomalies over the central to eastern extra-tropical Atlantic, in correspondence with the core of the positive SLP anomalies. The positive NAO is also associated with enhanced vertical westerly shear along ~20°N (Figs. 8c,g,k,o). The negative upper-level height anomaly (Figs. 8d,h) at ~30°N and associated upper-level westerly anomaly to the south of it is likely to drive this strong vertical westerly shear along ~20°N, contributing to very unfavorable conditions for TC genesis over the subtropical North Atlantic. Here again, the R8W run is the most realistic (with respect to R5W and NR) against the observed anomalies.

Figure 9 highlights the prominent role exerted by the AMM positive (negative) phase on favorable (unfavorable) conditions for TC genesis. In particular, negative SLP anomalies and drastic weakening of vertical westerly shear, which correspond to the positive phase, are conditions favorable to TC genesis over the western and central Atlantic (Figs. 9a,c,e,g,i,k,m,o) in agreement with Vimont and Kossin (2007), Kossin et al. (2010), Smirnov and Vimont (2011) and Patricola et al. (2014). Large positive RH700 anomalies over the subtropical Atlantic region (Figs. 9b,f,j,n) are associated with the AMM and are well reproduced in all experiments. However, a comprehensive verification of the experiments shows that, in general, the regressed AMM patterns resemble reasonably well the observations, with the R8W being by far the best (Fig. 9). Overall, Figs. 7-9 indicate that the R8W run provides the most realistic constraints on TC activity linked to the three large-scale climate modes, while also better reproducing the observed characteristics of the TC tracks (Figs. 2-5).

3.4 Reconstructing the interannual variations of atmospheric anomalies

The combined potential impacts of ENSO, the NAO and the AMM on Atlantic TC activity during each year is explored by creating a linear combination of the regressed anomalies and

corresponding PC time series. For example, the reconstructed $T_{ENSO}(x, y, t)$ for the ENSO mode at grid point (x,y) and time t is defined as

$$T_{ENSO}(x, y, t) = R_{ENSO}(x, y) \cdot TS_{ENSO}(t), \quad (2)$$

where $R_{ENSO}(x, y)$ is the regressed atmospheric field for the ENSO mode (1) and $TS_{ENSO}(t)$ is the normalized monthly PC time series for the ENSO mode. This procedure helps identify the effectiveness of these modes in reconstructing the observed atmospheric anomalies.

Figure 10 compares the observed SLP anomalies in 2005, 2006, 2010 and 2013 with the ones obtained in the experiments R8W and NR by combining the effects of ENSO, NAO and AMM modes. This comparison allows us to discern the model-produced atmospheric anomalies with and without the large-scale constraints (i.e., R8W versus NR). The R8W run (Figs. 10e-h) is particularly effective in reproducing the observed SLP anomalies (Figs. 10a-d) when the contributions of the three climate modes are acting together. In particular, the strong negative SLP anomaly over the central to western Atlantic which is indicative of enhanced TC genesis in 2005 (see Figs. 2a,c) is realistically reproduced (Figs. 10a,e). In the eastern Atlantic, the observed positive SLP anomaly is slightly hinted at in the R8W but totally missed in the NR (Fig. 10i), which leads to overestimated TC genesis in the NR over the region. In addition, the vast negative SLP anomaly joining the western tropical Atlantic with the mid latitude northeastern Atlantic is consistent with the typical path of early recurvers (non-landfalling TCs) which occur in the NR more than in the observations and R8W run (Figs. 2c,d).

Positive SLP anomalies characterize both the R8W and NR in 2006, consistent with reduced TC genesis, although the SLP zonal gradients in the central Atlantic are better characterized in the R8W.

In complete contrast with 2006, in 2010 the North Atlantic was characterized by a negative

SLP anomaly over most of the domain, with a positive SLP anomaly in the eastern mid-latitudes (see section 3.1, and Figs. 4a,c). The SLP anomaly pattern is again successfully captured by the R8W run (compare Figs. 10c,g,k). While the synergy of weak El Niño and near-neutral AMM in 2006 contribute to the positive SLP anomaly (see the impact of El Niño and the positive AMM on the SLP shown in Figs. 7a and 9a) over the western Atlantic and negative anomaly over the eastern Atlantic, the pattern in 2010 is reversed with a synergy between La Niña and a positive AMM phase, which lead to enhanced activity over the western Atlantic.

In spite of the Niño index being negative in both 2010 and 2013, the SLP distribution between the two is very different. While the negative Niño index caused positive SLP anomalies over the tropical eastern Pacific in both years (larger in 2010 than in 2013), the Atlantic region was dominated by a negative SLP anomaly in 2010 and by a positive SLP anomaly in 2013 (compare Figs. 10c and 10d). The positive SLP anomaly over the Atlantic in 2013 can be explained by the presence of a positive NAO, strong enough to counteract the effects of the neutral ENSO with weak negative Niño indices, as will be discussed later in the context of Table 3. As in the other cases, the R8W reproduces the anomalies over the subtropical North Atlantic (Figs. 10d,h), better than the NR.

We next extend our investigation to include the vertical wind shear and relative humidity fields (Fig. 11). While shear is often assumed to be westerly, easterly shear is also important, particularly at the early phases of TC genesis. Strong westerly shear can dissipate a mature hurricane, but easterly shear, even when moderate, can inhibit or delay the transformation of an open easterly wave into a closed circulation. Figures 11a,e,i suggest that the combined impacts of ENSO, the AMM, and the NAO lead to wetter conditions and weakening of vertical westerly shear over the Caribbean and western Atlantic during 2005, consistent with enhanced TC genesis

394 over the region and reduced number of Cape Verde systems over the eastern Atlantic (Fig. 2a
395 and Fig. 10a). During 2006, a positive vertical westerly shear anomaly is found between 10°-
396 20°N, along with a weak negative humidity anomaly over the western-central tropical Atlantic,
397 in both the observations and the R8W run (Figs. 11b,f). The NR run, in contrast, produces a
398 positive humidity anomaly over the Gulf of Mexico and subtropical Atlantic (Fig. 11j). In 2010,
399 the overall weakeness of vertical westerly shear over the subtropical North Atlantic suggest
400 strong TC activity including Cape Verde systems. These patterns are captured well in the R8W
401 and, to a lesser extent, in the NR (Figs. 11c,g,k).

402 Finally, the very inactive 2013 season, in spite of being a weak negative Niño index year, is
403 perhaps the most interesting case to demonstrate the importance of the combined action of the
404 three modes. Figure 11d indicates that 2013 was characterized by moderate to strong vertical
405 westerly shear throughout the entire tropical Atlantic, with dry conditions as well over the central
406 Atlantic. These patterns, according to Fogarty and Klotzbach (2014), may have contributed to the
407 poor skill of most operational seasonal TC forecasts. The R8W run was able to reproduce the
408 strong westerly wind shear and dry condition over the subtropical Atlantic (~20°N) (Figs. 11d,h)
409 except the very dry area over the central Atlantic between 10-15°N (Fig. 11d), suggesting other
410 contributing forcings. The NR could not reproduce the observed shear and humidity distributions
411 successfully, resulting in unrealistic TC track patterns (Fig. 5).

412

413 3.5 Relative contribution of the leading modes to seasonal anomalies

414 Figures 10 and 11 suggest that the interannually changing characteristics of the seasonal
415 atmospheric anomalies can be at least partially controlled by the interaction of the three leading
416 modes of variability. In order to examine the relative contributions of each mode, SLP, z250,

wind shear, and RH700 are reconstructed from the individual climate modes for each year, and then we calculate spatial correlations between the observed anomalies (e.g., left panels in Figs. 10 and 11) and model-reconstructed anomalies corresponding to each mode (see Table 3). The results reveal a prominent role of the AMM in 2005. In fact, the correlations with observation are highest for all four variables when the AMM is considered for reconstruction (see 3–6th rows and 3–6th columns in Table 3). Specifically, favorable conditions for TC genesis and tracks over the western Atlantic and Gulf of Mexico resulting from strong negative SLP (Fig. 10a), weakening of westerly shear (Fig. 11a), and positive humidity (Fig. 11a) anomalies can be largely linked to the positive SSTs caused by a strong positive AMM over that region. The atmospheric anomalies forced by the tropical eastern Pacific SST, which was almost bordering near-neutral ENSO conditions (see Fig. 6d), show a negative or weak positive correlation with the observations (3rd row and 3–6th columns in Table 3), suggesting that the ENSO impact is overwhelmed by the strong positive AMM. This relative influence of ENSO and AMM appears very important to explain seasonal Atlantic TC activity (Patricola et al. 2014).

The ENSO signal (El Niño) in 2006 (Fig. 6d) is more important in characterizing the atmospheric anomalies than in 2005. However, since the 2006 El Niño was not a strong event, its impact does not stand out among the three modes in accounting for the seasonal atmospheric patterns during that year (7–10th rows and 3–6th columns in Table 3). We can speculate that the TC activity during 2006 can be understood as the combined effect of the weak El Niño, neutral NAO, and neutral AMM in summer, and possibly other forcings not included in this work such as unusual dust activity (Lau and Kim 2007).

The active hurricane season of 2010 is found to be significantly correlated with ENSO and the AMM. All four variables constructed from La Niña (Fig. 6d) or the positive AMM (Fig. 6f)

440 are more highly correlated with the observations than the negative NAO. However, the negative
441 phase of the NAO exerts some control on the TC track patterns, which are very different from
442 the other active TC season of 2005. While the impact of the strong positive AMM phase is
443 comparable in 2005 and 2010, Fig. 12 shows that the impact of the ENSO and NAO modes is
444 drastically different. Fig. 12a suggests that the neutral ENSO and positive NAO in 2005 produce
445 weak positive SLP anomalies over the Atlantic, notwithstanding a substantial positive AMM-
446 induced modification in 2005. In contrast, the impacts of the La Niña and negative NAO in 2010
447 produce negative SLP anomalies (Fig. 12b) and positive SST anomalies (Figs. 12d) over the
448 entire subtropical Atlantic. This impact, combined with the positive AMM, further enhances the
449 negative SLP and positive SST anomalies over the subtropical Atlantic. The above differences in
450 the climate anomalies may explain why TC genesis was mainly confined to the western Atlantic
451 in 2005, with very few Cape Verde systems, in contrast with 2010.

452 Correlations for the 2013 hurricane season indicate a significant contribution of the NAO to
453 the observed anomaly distributions. While the other two modes were weak in magnitude, the
454 impact of the positive NAO (known to weaken TC genesis over the North Atlantic - Knaff
455 (1997) and Kossin et al. (2010)) appeared to exert strong control in developing conditions
456 unfavorable to TC activity (see also
457 http://www.srh.noaa.gov/bro/?n=2013event_hurricaneseasonwrap). Table 3 shows that the
458 correlations between observations and the reconstructed variables based on the NAO are greatest
459 (15–18th rows and 3–6th columns in Table 3) without exception, with the other two modes
460 having much lower correlations with observations. This argument appears connected with Zhang
461 et al. (2016) that suggested the role of strong anti-cyclonic Rossby wave breaking, which tends
462 to be more active during the positive NAO phase (Riviére et al. 2010) and could have

463 contributed to equatorward intrusion of extratropical dry air especially in August and September
464 in 2013, leading to poor conditions for TC activity.

465 Consistent with previous findings, the NR results are relatively poor when compared to the
466 R8W (3rd–6th vs 7–10th columns in Table 3). Although the NR run is successful in reproducing
467 the interannual variation of the TC genesis frequency, it is not so successful in reproducing the
468 spatial structure of the three dominant modes, their interannual variation of phase and intensity,
469 and the associated seasonal TC track patterns for each year.

470

471 3.6 TC genesis frequency statistics associated with the MJO

472 An additional question addressed in this section is whether the simulations that constrain the
473 atmospheric planetary-scales larger than ~5,000 km wavelength (corresponding to R8W) can
474 realistically capture the Atlantic TC genesis frequency statistics, known to depend on the phase
475 of the MJO (Maloney and Hartmann 2000; Camargo et al. 2009; Kossin et al. 2010; Klotzbach
476 2010). To this purpose, the timing of the TC genesis associated with the phase of MJO is
477 examined by counting the TC genesis dates from observations, R5W run, and R8W run with
478 respect to the MJO phases using the Wheeler and Hendon (2004) MJO indices. The
479 observationally-based results (Table 4) reveal that TC genesis tends to be most active when the
480 MJO-enhanced convection with tropical westerlies occurs in the western hemisphere (phase 1
481 and 8, Wheeler and Hendon 2004), while TC genesis becomes inactive when the MJO-enhanced
482 convection occurs over the western Pacific (phase 6 and 7), consistent with Maloney and
483 Hartmann (2000) and Klotzbach and Oliver (2015). This characteristic feature of the MJO is
484 reproduced better in R8W than in R5W, demonstrating that atmospheric scales between 8000km
485 and 5000km are very important to realistically explain the TC genesis frequency statistics

associated with the MJO phase.

3.7 Predicting the large-scale impacts of ENSO, NAO, and AMM

The previous results consistently indicate that the unconstrained NR cannot reproduce the planetary scale atmospheric features important for TC seasonal prediction. In this section, the issue of SST-based predictability of relevant atmospheric variations associated with the three leading modes (ENSO, NAO, and AMM) is investigated with the aid of the GEOS-5 AGCM forced with observed SSTs. To this purpose, an ensemble of twenty NRs was produced for each of the nine TC seasons (2005-2013). The ensemble members differ only in the atmospheric/land initial conditions taken from MERRA for May 1 to May 20 of each year. The predictability of the individual modes is assessed in terms of signal to noise (S/N) ratios for SLP and z250. The SLP and z250 distributions associated with the ENSO, NAO, and AMM modes are identified and then the interannual variations of these modes are examined for each ensemble member.

The left panel in Fig. 13 shows the z250 anomalies associated with the three modes, respectively. The light-green contours are the results for each ensemble member. The results show considerable scatter among the members, especially over mid-latitude region (say north of 25°N). The ensemble mean anomalies represented by black contours do, however, resemble the typical observed z250 anomaly distributions associated with the positive phase of the ENSO, NAO, and AMM modes (cf. Figs. 13a,b,c with Figs. 7d,8d,9d). However, the PC time series shown in the right panel of Fig. 13 reveal large uncertainty in the interannual variation of the phase of the ENSO and NAO modes. This large ensemble spread indicates that predictability of these two major modes of variability impacting TC activity is low on seasonal time scales in summer, though we cannot rule out the possibility that this reflects model errors. Particularly, the

large uncertainty associated with ENSO seems to be due to inconsistent extra-tropical responses to the ENSO forcing among the members. The uncertainty is significantly reduced when we focus on the tropical region only (e.g., tropical Atlantic and eastern Pacific) for capturing the ENSO mode (Figure not shown) (see also high S/N ratios over the tropics in Figs. 14a,d). Compared to ENSO and the NAO, the predictability of the AMM is considerably higher as all ensemble members exhibit similar variations, in good agreement with the observed values (Fig. 13f).

The distribution of the S/N ratio of the monthly variation of the ENSO, NAO, and AMM modes is shown in Fig. 14. The S/N ratio increases with a decrease in variance of intra-ensemble differences (i.e., residual variance). The S/N ratios for ENSO reveal that the highest SLP S/N ratio is found over the eastern tropical Pacific. The low-latitudes of the Atlantic region exhibit the second highest S/N ratios. This includes the Gulf of Mexico, part of the Caribbean Sea and the eastern subtropical Atlantic, where many TCs are typically generated. The predictability of z250 associated with the ENSO signal is high (> 0.8) over the low-latitude Atlantic basin. The Caribbean Sea region has the largest S/N ratio, exceeding 0.9 (Fig. 14d).

The predictability of the NAO-related response is found to be relatively low. Figure 14b shows that the highest S/N ratios for SLP are limited to the eastern tropical Pacific and the Caribbean Sea. The S/N ratios for z250 suggest that relatively high predictability occurs in a belt confined to ~20°N (Fig. 14e), with S/N values in other regions between zero and 0.2.

The predictability of the AMM represented by z250 is found to be higher than the one associated with ENSO over low-latitudes (compare Figs. 14d,f). Figure 14f shows that the S/N ratio is close to 1 within +/- 20° of the equator. However, the S/N ratio drops rapidly to values smaller than 0.2 to the north of 40°N. The predictability of the AMM in terms of SLP is higher

532 over the tropical eastern Pacific and the western Atlantic including the Caribbean Sea (Fig. 14c).

533 Figures 13 and 14 suggest that predictive skill of the primary large-scale modes of
534 variability of the atmosphere is to a large extent limited to the tropical to sub-tropical regions.
535 This is particularly true for the NAO. Whether this represents a realistic estimate of intrinsic
536 atmospheric predictability on seasonal time scales (linked to SST), or whether this partly reflects
537 a limitation of the GEOS-5 AGCM is yet to be determined. Extra-tropical weather patterns,
538 affected by transient dynamical forcings which have generally larger amplitudes than the tropical
539 ones, may contribute to the relatively low NAO predictability. It is likely that the extra-tropical
540 North Atlantic region, dominated by baroclinic activity, needs additional investigation to
541 improve prediction of the largest planetary-scales.

542

543 4. Concluding remarks and discussion

544 This study examined the impact of the large-scale climate modes on seasonal Atlantic TC
545 activity by focusing on genesis frequency, genesis locations, and overall track patterns and
546 landfalls. A particular focus was on the unexpected TC activity that occurred in recent several
547 years (e.g., 2005, 2006, 2010 and 2013). Both observational analysis and climate model
548 simulations were conducted to better understand the large-scale climate modes that impact
549 Atlantic TC activity on seasonal time scales. Three leading well-known climate modes were
550 identified consisting of ENSO, the NAO and the AMM. It was found that a substantial amount
551 of the variability in the observed mass fields (SLP and upper-level geopotential height (z250)),
552 vertical wind shear, and relative humidity over the North Atlantic can be reproduced as a linear
553 combination of these three modes, highlighting the important role they play in impacting year-to-
554 year changes in seasonal TC activity.

In spite of the general relationship between the Atlantic TC genesis frequency and ENSO (Bove et al. 1998; Elsner and Bossak 2001; Klotzbach 2011), there have been several years with active TC genesis during the warm ENSO and inactive TC genesis during cold ENSO. In this study, it was suggested that the counter-intuitive TC activity that occurred in 2005 and 2013 is the result of the strong impact of a positive AMM in 2005 and a positive NAO in 2013, which acted to modify the impact of ENSO. A positive AMM caused warmer SSTs to occur over the western and central Atlantic in 2005, leading to more favorable conditions for active TC genesis in that region compared to that in the eastern Atlantic, and more landfalls over the US. For the case of a weak TC season in 2013, the strong impact of a positive NAO overwhelmed a weak negative Niño SST impact, producing a positive SLP anomaly over the Atlantic, stronger vertical westerly shear, and drier atmosphere (~700hPa) over the Atlantic TC genesis region. As such, this year was strongly impacted by the extratropics, unlike the other years that were primarily controlled by the changes in the low-latitude Atlantic (e.g., tropical SST).

For the case of 2010, widespread negative SLP anomalies occurred over the subtropical Atlantic due to the combined influence of La Niña, a negative NAO and a positive AMM, providing very favorable conditions for TC genesis over that region. The impact of the three modes was to also produce an expanded area of positive SST anomalies across the low-latitudes of the Atlantic and a weak westward expansion of the North Atlantic subtropical high, leading to more early recurvers and fewer landfalling systems over the US, despite it being an active TC year. The 2006 TC season also appears to be controlled by a synergy of the three modes in producing the seasonal atmospheric anomalies that drove the weak TC activity. Additionally, a TC-suppressing role attributed by other authors to anomalous dust production and reduced SSTs in 2006 (Lau and Kim 2007), not investigated in this work, should be taken into account.

578 This study also found that, in general, the large-scale atmospheric variability over the
579 subtropical North Atlantic with wavelengths approximately greater than 4,000–5,000km, which
580 is much larger than the typical horizontal scale of TCs, is responsible for controlling the changes
581 in North Atlantic TC activity on seasonal time scales. In fact, those scales are sufficient to
582 faithfully account for the relevant spatio-temporal variations of ENSO, the NAO, and the AMM.
583 Our analysis reveals that the seasonal atmospheric anomalies during any particular year are very
584 sensitive to the phase and intensity of these modes. As such, the combined impact of these modes
585 can produce seasonal TC activity that is opposite to the conventional understanding about the
586 impact of any of the leading modes alone (e.g., strong TC activity during a neutral ENSO and
587 positive NAO in 2005, and weak TC activity during weak negative Niño index in 2013). This
588 study suggests that while ENSO is very important, its interaction with the AMM and NAO (and
589 perhaps other forcings) in modulating the Atlantic TCs appears to provide a more robust
590 explanation of TC interannual variability.

591 A caveat for this study is that the impact of the Atlantic Multi-decadal Oscillation (AMO)
592 (Klotzbach 2011; Caron et al. 2014), also known to be important for influencing Atlantic TC
593 activity on decadal time scales (a positive AMO, characterized by positive Atlantic SST
594 anomalies, is associated with more intense hurricanes), is not included in this work. Vimont and
595 Kossin (2007) suggest that the impact of the AMO on seasonal TC activity manifests itself
596 through the AMM because the AMO can excite the AMM on decadal time scales. The AMO has
597 been in the positive phase for our analysis period (2005-2013), thus possibly enhancing Atlantic
598 TC activity. However, the AMO index was only slightly positive during the late spring in 2013.
599 Fogarty and Klotzbach (2014) suggest that AMO weakening on subseasonal time scale might
600 have a delayed TC suppressing impact in 2013, interacting with the extra-tropical impact by the

positive phase of the NAO.

This study contributes to the understanding of TC predictability on seasonal and subseasonal scales by showing evidence that phase and intensity of the AMM are more predictable, followed by ENSO, particularly over low latitudes. The predictive skill for both modes declines towards the mid latitudes, where the response to the AMM or ENSO tends to be inconsistent among different ensemble members, implying larger uncertainty. An even more challenging aspect of the TC prediction problem is the relatively low predictability of NAO because of its intrinsically shorter time scales and greater association with the mid-latitude dynamics. As a future and challenging step towards increased TC predictability on a subseasonal scale, inclusive of track and landfall distributions, a more advanced understanding of the NAO will be necessary.

Acknowledgements

This work is supported by the NASA Modeling, Analysis, and Prediction (MAP) Program (Award number: 802678.02.17.01.29). The authors are grateful to anonymous reviewers for their helpful comments and suggestions.

References

Aiyyer, A. R., and C. Thorncroft, 2006: Climatology of vertical wind shear over the tropical Atlantic. *J. Climate*, **19**, 2969-2983.

Barnston, A. G., and R. E. Livezey, 1987: Classification, seasonality and persistence of low-frequency atmospheric circulation pattern. *Mon. Wea. Rev.*, **115**, 1083-1126.

Bacmeister, J. T., M. J. Suarez, and F. R. Robertson, 2006: Rain reevaporation, boundary layer–convection interactions, and Pacific rainfall patterns in an AGCM. *J. Atmos. Sci.*, **63**, 3383–3403.

Bacmeister, J. T., M. F. Wehner, R. B. Neale, A. Gettelman, C. Hannay, P. H. Lauritzen, J. M. Caron, and J. E. Truesdale, 2014: Exploratory high-resolution climate simulations using the Community Atmosphere Model (CAM). *J. Climate*, **27**, 3073-3099.

Bell, G. D., E. S. Blake, T. B. Kimberlain, C. W. Landsea, J.-K. E. Schemm, R. J. Pasch, and S. B. Goldenberg, 2011: State of the climate 2010. *Bull. Amer. Meteor. Soc.*, **92(6)**, S115-120.

Blake E. S., and E. J. Gibney, 2011: The deadliest, the costliest, and most intense United States tropical cyclones from 1851 to 2010 (and other frequently requested hurricane facts). NOAA Technical Memorandum NWS NHC-6, 47pp.

Blake, E. S., National Hurricane Center Annual Summary. 2013 Atlantic Hurricane Season, 9pp. Available at http://www.nhc.noaa.gov/data/tcr/summary_atlc_2013.pdf

Bloom, S., L. Takacs, A. DaSilva, and D. Ledvina, 1996: Data assimilation using incremental analysis updates. *Mon. Wea. Rev.*, **124**, 1256-1271.

Bove, M. C., J. J. O'Brien, J. B. Eisner, C. W. Landsea, and X. Niu, 1998: Effect of El Niño on U.S. landfalling hurricanes, revisited. *Bull. Amer. Meteor. Soc.*, **79**, 2477–2482.

Camargo, S. J., K. Emanuel, and A. Sobel, 2007: Use of a genesis potential index to diagnose ENSO effects on tropical cyclone genesis. *J. Climate*, **20**, 4819-4834.

Camargo, S. J., M. C. Wheeler, and A. H. Sobel, 2009: Diagnosis of the MJO modulation of tropical cyclogenesis using and empirical index. *J. Atmos. Sci.*, **66**, 3061-3074, doi: 10.1175/2009JAS3101.1.

Caron, L.-P., M. Boudreault, and C. L. Bruyère, 2014: Changes in large-scale controls of Atlantic tropical cyclone activity with the phases of the Atlantic multidecadal oscillation. *Clim. Dyn.*, doi: 10.1007/s00382-014-2186-5.

Chen, J.-H., and S.-J. Lin, 2013: Seasonal Predictions of Tropical Cyclones Using a 25-km Resolution General Circulation Model. *J. Climate*, **26**, 380-398, doi:10.1175/JCLI-D-12-00061.1.

Chiang, J. C. H., and D. J. Vimont, 2004: Analagous meridional modes of atmosphere-ocean variability in the tropical Pacific and tropical Atlantic. *J. Climate*, **17**, 4143-4158.

Colbert, A. J., and B. J. Soden, 2012: Climatological variations in North Atlantic tropical cyclone tracks. *J. Climate*, **25**, 657-673, doi: 10.1175/JCLI-D-11-00034.1.

Deser, C., M. A. Alexander, S.-P. Xie, and A. S. Phillips, 2010: Sea surface temperature variability: Patterns and mechanisms. *Annu. Rev. Mar. Sci*., 115-143.

Elsner, J. B., and B. H. Bossak, 2001: Secular changes to the ENSO-U.S. hurricane relationship. *Geophys. Res. Lett*., **28(21)**, 4123-4126.

Elsner, J. B., 2003: Tracking hurricanes. *Bull. Amer. Meteor. Soc*., **84**, 353–356.

Elsner, J. B., and T. Jagger, 2006: Prediction models for annual US Hurriane counts. *J. Climate*, **19,** 2935-2952.

Fogarty, C. T., and P. Klotzbach, 2014: The 2013 Atlantic hurricane season: blip or flip? *Bull. Amer. Meteor. Soc*., **95(7)**, S106-107.

Gelaro, R., and co-authors, 2015: *Evaluation of the 7-km GEOS-5 Nature Run*. NASA Technical Report Series on Global Modeling and Data Assimilation, NASA/TM-2014-104606, **36**. 305 pp.

Knaff, J. A., 1997: Implications of summertime sea level pressure anomalies in the tropical Atlantic region. *J. Climate*, **10**, 789–804.

Kim, H.-M., and P. J. Webster, 2010: Extended-range seasonal hurricane forecasts for the North Atlantic with a hybrid dynamical-statistical model. Geophys. Res. Lett., 37, L21705, doi:10.1029/2010GL044792.

Klotzbach, P. J., and W. M. Gray, 2004: Updated 6-11-month prediction of Atlantic basin seasonal hurricane activity. *Wea. Forecasting*, **19**, 917-934.

Klotzbach, P. J., 2010: On the Madden-Julian Oscillation-Atlantic hurricane relationship. *J. Climate*, **23**, 282-293, doi: 10.1175/2009JCLI2978.1.

Klotzbach, P. J., 2011: The influence of El Niño-Southern Oscillation and the Atlantic multidecadal oscillation on Caribbean tropical cyclone activity. *J. Climate*, **24**, 721-731, doi: 10.1175/2010JCLI3705.1.

Klotzbach, P. J., and E. C. J. Oliver, 2015: Modulation of the Atlantic basin tropical cyclone activity by the Madden-Julian Oscillation (MJO) from 1905 to 2011. *J. Climate*, **28**, 204-217, doi: 10.1175/JCLI-D-14-00509.1.

Knutson, T. R., J. J. Sirutis, S. T. Garner, I. M. Held, and R. E. Tuleya, 2007: Simulation of the recent multidecadal increase of Atlantic hurricane activity using an 18-km-grid regional model. B*ull. Amer. Meteor. Soc.*, **88**, 1549–1565.

Kossin, J. P., and D. J. Vimont, 2007: A more general framework for understanding Atlantic hurricane variability and trends. *Bull. Amer. Meteor. Soc.*, **88**, 1767-1781.

Kossin, J. P., and S. J. Camargo, 2009: Hurricane track variability and secular potential intensity trends. *Climate Change*, **97**, 329-337, doi:10.1007/s10584-009-9748-2.

Kossin, J. P., S. J. Camargo, and M. Sitkowski, 2010: Climate modulation of North Atlantic hurricane tracks. *J. Climate*, **23**, 3057-3076.

Koster, R. D., M. J. Suarez, A. Ducharne, M. Stieglitz, and P. Kumar, 2000: A catchment-based approach to modeling land surface processes in a general circulation model: 1. Model structure. *J. Geophys. Res.*, **105**, 24809–24822, doi:10.1029/2000JD900327.

Landsea, C. W., and J. L. Franklin, 2013: Atlantic hurricane database uncertainty and presentation of a new database format. *Mon. Wea. Rev.*, **141**, 3576-3592, doi: 10.1175/MWR-D-12-00254.1.

LaRow, T. E., Y.-K. Lim, D. W. Shin, S. Cocke, and E. P. Chassignet, 2008: Atlantic basin seasonal hurricane simulations. *J. Climate*, **21**, 3191-3206, doi:10.1175/2007JCLI2036.1.

Larson, J., Y. Zhou, and R. W. Higgins, 2005: Characteristics of landfalling tropical cyclones in the United States and Mexico: Climatology and interannual variability. *J. Climate*, **18**, 1247–1262.

Lau, K.-M., and K. M. Kim, 2007: Cooling of the Atlantic by Saharan dust. *Geophys. Res. Lett.*, **34**, L23811, doi:10.1029/2007GL031538.

Lim, Y.-K., S. D. Schubert, O. Reales, M.-Y. Lee, A. M. Molod, and M. J. Suarez, 2015: Sensitivity of tropical cyclones to parameterized convection in the NASA GEOS5 model. *J. Climate*, **28(2)**, 551-573, doi:10.1175/JCLI-D-14-00104.1.

Lin, S.-J., 2004: A vertically Lagrangian finite-volume dynamical core for global models. *Mon. Wea. Rev.*, **132**, 2293–2307.

Maloney, E. D., and D. L. Hartmann, 2000: Modulation of hurricane activity in the Gulf of Mexico by the Madden-Julian Oscillation. *Science*, **287**, 2002-2004.

Mo, K. C., 2000: The association between intraseasonal oscillations and tropical storms in the Atlantic basin. *Mon. Wea. Rev*., **128**, 4097-4107.

Molod, A., L. Takacs, M. Suarez, J. Bacmeister, I.-S. Song, and A. Eichmann, 2012: The GEOS-5 Atmospheric General Circulation Model: Mean Climate and Development from MERRA to Fortuna. *NASA Technical Report Series on Global Modeling and Data Assimilation, NASA TM—2012-104606,* **28**, 117 pp.

Moorthi, S., and M. J. Suarez, 1992: Relaxed Arakawa-Schubert: A parameterization of moist convection for general circulation models. *Mon. Wea. Rev*., **120**, 978-1002.

Murakami, H., G. A. Vecchi, S. Underwood, T. L. Delworth, A. T. Wittenberg, W. G. Anderson, J.-H. Chen, R. G. Gudgel, L. M. Harris, S.-J. Lin, and F. Zeng, 2015: Simulation and prediction of category 4 and 5 hurricanes in the high-resolution GFDL HiFLOR coupled climate model. *J. Climate*, **28**, 9058-9079, doi: 10.1175/JCLI-D-15-0216.1.

O'Brien, J. J., T. S. Richards, and A. C. Davies, 1996: The effect of El Niño on U.S. landfalling hurricanes. *Bull. Amer. Meteor. Soc*. **77**, 773-774.

Patricola, C. M., R. Saravanan, and P. Chang, 2014: The impact of the El Niño-Southern Oscillation and Atlantic meridional mode on seasonal Atlantic tropical cyclone activity. J. Climate, 5311-5328, doi: 10.1175/JCLI-D-13-00687.1.

Putman, W. M., and M. Suarez. 2011: Cloud-system resolving simulations with the NASA Goddard Earth Observing System global atmospheric model (GEOS-5). *Geophys. Res. Lett.*, **38(16)**, L16809, doi:10.1029/2011GL048438.

Rayner, N. A., and Coauthors, 2003: Global analyses of sea surface temperature, sea ice, and night time air temperature since the late nineteenth century. *J. Geophys. Res*., **108,** (D14), 4407, doi:10.1029/2002JD002670.

Reale, O., W. K. Lau, J. Susskind, E. Brin, E. Liu, L. P. Riishojgaard, M. Fuentes, and R. Rosenberg, 2009: AIRS impact on the analysis and forecast track of tropical cyclone Nargis in a global data assimilation and forecasting system. *Geophys. Res. Lett*., **36**, L06812, doi:10.1029/2008GL037122.

Reed, K. A., and C. Jablonowski, 2011: Impact of physical parameterizations on idealized tropical cyclones in the Community Atmosphere Model. *Geophys. Res. Lett*., **38**, L04805, doi:10.1029/2010GL046297.

Rienecker M. M. and Coauthors, 2008: The GEOS-5 data assimilation system – documentation of versions 5.0.1 and 5.1.0, and 5.2.0. In: NASA technical report series on global modeling and assimilation, NASA/TM-2008-104606, **27**, 92pp.

Rienecker, M.M., and Coauthors, 2011: MERRA - NASA's Modern-Era Retrospective Analysis for Research and Applications. *J. Climate*, **24**, 3624-3648. doi: 10.1175/JCLI-D-11-00015.1.

Rivière, G., A. Laîné, G. Lapeyre, D. Salas-Mélia, and M. Kageyama, 2010: Links between Rossby wave breaking and the North Atlantic oscillation–Arctic oscillation in present-day and last glacial maximum climate simulations. *J. Climate*, **23**, 2987–3008, doi:10.1175/2010JCLI3372.1.

Shaman, J., S. K. Esbensen, and E. D. Maloney, 2009: The dynamics of the ENSO-Atlantic hurricane teleconnection: ENSO-related changes to the North African-Asian jet affect Atlantic basin tropical cyclogenesis. *J. Climate*, **22**, 2458-2482.

Smirnov, D., and D. J. Vimont, 2011: Variability of the Atlantic meridional mode during the Atlantic hurricane season. *J. Climate*, **24**, 1409-1424, doi: 10.1175/2010JCLI3549.1.

Smith, S. R., J. Brolley, J. J. O'Brien, and C. A. Tartaglione, 2007: ENSO's impact on regional U.S. hurricane activity. *J. Climate*, **20**, 1404–1414.

Tartaglione, C. A., S. R. Smith, and J. J. O'Brien, 2003: ENSO impact on hurricane landfall probabilities for the Caribbean. *J. Climate*, **16**, 2925–2931.

Tokioka, T., K. Yamazaki, A. Kitoh, and T. Ose, 1988: The equatorial 30–60 day oscillation and the Arakawa-Schubert penetrative cumulus parameterization, *J. Meteorol. Soc. Japan*., **66**, 883–901.

Vecchi, G. A., and coauthors, 2014: On the seasonal forecasting of regional tropical cyclone activity. *J. Climate*, **27**, 7994-8016, doi: 10.1175/JCLI-D-14-00158.1.

Vimont, D. J., and J. P. Kossin, 2007: The Atlantic meridional mode and hurricane activity. *Geophys. Res. Lett*., **34**, L07709, doi: 10.1029/2007GL029683.

Vitart, F., D. Anderson, and T. Stockdale, 2003: Seasonal forecasting of tropical cyclone landfall over Mozambique. *J. Climate*, **16**, 3932-3945.

766 Wallace, J. M., and D. S. Gutzler, 1981: Teleconnections in the geopotential height field during
767 the Northern Hemisphere winter. *Mon. Wea. Rev*., **109**, 784–812.
768 Walsh, K. J. E., M. Fiorino, C. W. Landsea, and K. L. McInnes, 2007: Objectively determined
769 resolution-dependent threshold criteria for the detection of tropical cyclones in climate
770 models and reanalyses. *J. Climate*, **20**, 2307–2314.
771 Wang, C., H. Liu, S.-K. Lee, and R. Atlas, 2011: Impact of the Atlantic warm pool on United
772 States landfalling hurricanes. *Geophys. Res. Lett.*, **38**, L19702, doi:10.1029/2011GL049265.
773 Wang, Z., G. Zhang, M. S. Peng, J.-H. Chen, and S.-J. Lin, 2015: Predictability of Atlantic
774 Tropical Cyclones in the GFDL HiRAM Model. *Geophys. Res. Lett.*, **42(7)**,
775 doi:10.1002/2015GL063587.
776 Wheeler, M. C., and H. H. Hendon, 2004: An all-season real-time multivariate MJO index:
777 Development of an index for monitoring and prediction. *Mon. Wea. Rev*., **132**, 1917-1932.
778 Xie, L., T. Yan, L. J. Pietrafesa, J. M. Morrison, and T. Karl, 2005: Climatology and interannual
779 variability of North Atlantic hurricane tracks. *J. Climate*, **18**, 5370-5381.
780 Zhang, G., Z. Wang, T. Dunkerton, M. Peng, and G. Magnusdottir, 2016: Extratropical impacts
781 on Atlantic tropical cyclone activity. *J. Atmos. Sci*, in press.
782 Zhao, M., I. M. Held, S.-J. Lin, and G. A. Vecchi, 2009: Simulations of global hurricane
783 climatology, interannual variability, and response to global warming using a 50-km
784 resolution GCM. *J. Climate*, **22**, 6653-6678, doi:10.1175/2009JCLI3049.1.
785 Zhao, M., I. M. Held, and S.-J. Lin, 2012: Some counter-intuitive dependencies of tropical
786 cyclone frequency on parameters in a GCM. *J. Atmos. Sci.*, **69(7)**, 2272-2283,
787 doi:10.1175/JAS-D-11-0238.1.
788 Zhu, X., R. Saravanan, and P. Chang, 2012: Influence of mean flow on the ENSO-vertical wind
789 shear relationship over the northern tropical Atlantic. J. Climate, 25, 858-864, doi:
790 10.1175/JCLI-D-11-00213.1.

Table 1. List of the threshold values for detecting the TC using the detection/tracking algorithm based on Vitart et al. (2003)

Variables	local relative vorticity maximum (850hPa)	warm core temperature maximum	minimum sea level pressure (SLP)	minimum lower-level wind speed	minimum duration
Criteria	$3.5 \times 10^{-5}\ s^{-1}$	Distance between the TC center and the center of the warm core must not exceed 2° lon.&lat.	Minimum SLP defines the TC center and must exist within 2°×2° radius of the vorticity maximum	$12m\ s^{-1}$	2 days

Table 2. TC track density and the number of TC landfalls (numbers in parentheses) averaged over the continental 1) US and Canada, and 2) Mexico and Central America. Results from observations are shown in the third column, while three ensemble member mean results for R5W, R8W, and NR, respectively, are shown in 4–6th columns. TC track density and landfalling TC counts are calculated for each hurricane season (2005, 2006, 2010, and 2013).

		TC track density (landfalls)			
		Obs.	R5W	R8W	NR
2005	US and Canada	0.58 (6)	0.49 (4.7)	0.54 (5)	0.36 (3.7)
	Mexico and Central America	1.27 (5)	0.69 (1)	1.28 (1.7)	1.18 (2)
2006	US and Canada	0.26 (2)	0.18 (2.7)	0.20 (1.7)	0.25 (3.3)
	Mexico and Central America	0.0 (0)	0.39 (0.3)	0.37 (0.7)	0.53 (1.7)
2010	US and Canada	0.13 (2)	0.18 (2.7)	0.16 (1.7)	0.47 (5.3)
	Mexico and Central America	1.26 (6)	1.63 (2.7)	1.09 (3)	1.71 (4)
2013	US and Canada	0.25 (1)	0.16 (1.3)	0.09 (2)	0.35 (3.7)
	Mexico and Central America	1.13 (2)	0.33 (0.7)	0.47 (1.7)	0.73 (2)

Table 3. Spatial correlations between observed anomaly distribution (left panels in Figs. 10 and 11) and distribution of reconstructed model-anomalies associated with the phase and intensity of the ENSO, NAO, and AMM, respectively. Spatial correlations are calculated for each hurricane season (2005, 2006, 2010, and 2013). The observed phases of each leading mode in each year are noted within parentheses in the second column. Variables considered for examining spatial correlations are SLP, z250, vertical wind shear (WS), and 700hPa relative humidity (RH).

		Obs. vs. R8W				Obs. vs. NR			
		SLP	z250	WS	RH	SLP	z250	WS	RH
2005	ENSO (0)	-0.02	-0.36	0.28	-0.02	-0.02	-0.06	0.01	0.27
	NAO (+)	0.43	0.34	0.06	0.18	-0.22	-0.37	0.05	-0.39
	AMM (+)	0.79	0.63	0.56	0.49	0.57	0.03	0.47	0.59
	E+N+A	0.71	0.63	0.56	0.50	0.20	0.01	0.42	0.59
2006	ENSO (+)	0.54	0.34	0.30	0.02	-0.09	0.63	0.35	0.07
	NAO (0)	0.30	0.58	0.26	0.01	0.10	0.48	0.25	0.11
	AMM (0)	0.58	0.19	0.39	0.03	0.63	-0.16	0.38	0.00
	E+N+A	0.70	0.45	0.35	0.01	0.10	0.61	0.48	0.08
2010	ENSO (–)	0.74	0.64	0.56	0.29	0.44	0.77	0.65	0.32
	NAO (–)	0.20	0.16	0.27	-0.06	0.23	0.22	0.39	0.31
	AMM (+)	0.58	0.78	0.71	0.46	0.30	-0.17	0.74	0.18
	E+N+A	0.86	0.88	0.92	0.51	0.41	0.34	0.79	0.40
2013	ENSO (0)	0.13	0.01	0.14	0.12	-0.18	-0.12	-0.47	-0.01
	NAO (+)	0.82	0.32	0.54	0.43	0.43	0.13	0.64	0.09
	AMM (+)	0.26	0.23	0.55	0.10	0.75	0.44	0.63	0.14
	E+N+A	0.85	0.31	0.46	0.15	0.40	-0.02	-0.14	0.04

Table 4 The number of TC genesis within different MJO phases (Wheeler and Hendon 2004). Phase 2 and 3, phase 4 and 5, phase 6 and 7, and phase 8 and 1 represents, respectively, the MJO-driven convection over the Indian Ocean, the Maritime Continents, the western North Pacific, and the western Hemisphere. Note that the number of TC genesis obtained from the R5W and the R8W data are the sum of all TCs in the three ensemble members.

	Phase 2 and 3	Phase 4 and 5	Phase 6 and 7	Phase 8 and 1
Obs.	17	17	8	25
R5W	53	45	26	52
R8W	58	45	21	67

Figure Captions

Figure 1. A schematic view of replaying the GEOS-5 model to an existing atmospheric analysis dataset. The process is generalized here to apply a filter to the full increments to allow constraining a subset of the flow.

Figure 2. TC tracks for 2005 for a) observations, b) R5W, c) R8W and d) NR. All TC tracks produced by three member runs are plotted for R5W, R8W, and NR. Shading represents the three-member-averaged SLP anomaly for 2005. Number in parentheses above each panel is the average number of detected TCs across the three members. Panels of e, f, and g are distribution of differences in TC track density between model and observation (a). Bottom panels (h, i, and j) are distribution of differences in TC genesis locations between model and observation (a).

Figure 3. Same as Figure 2 but for 2006.

Figure 4. Same as Figure 2 but for 2010.

Figure 5. Same as Figure 2 but for 2013.

Figure 6. The first three rotated empirical orthogonal functions (REOFs) of the observed monthly SST for summer (June to September). The left panel represents the distribution of non-normalized eigenvectors whereas the right panel represents the corresponding PC time series (black solid line). Time series in blue solid lines denote, from the top to bottom panel, the Niño3.4 SST (top), NAO index (middle) and AMM index multiplied by 0.5 (bottom).

Figure 7. Anomaly distributions of the SLP (top row), relative humidity at 700hPa (second row), vertical wind shear (u(150hPa) minus u(850hPa)) (third row) and height at 250hPa (bottom row) regressed onto ENSO. Hatching in the third row panels represents climatologically the easterly wind shear region from observations. Each panel from the left represents the result for observation (first), R8W (second), R5W (third), and NR (fourth).

Figure 8. Same as Figure 7 but for the NAO.

Figure 9. Same as Figure 7 but for the AMM.

Figure 10. Distribution of SLP anomaly resulting from the combined effect of the ENSO, NAO and AMM. From the top to bottom panel, each panel represents the result for 2005, 2006, 2010 and 2013. Each panel from the left represents the result for observation (left), R8W (middle), and NR (right).

Figure 11. Same as Figure 10 but for vertical wind shear (u(150hPa) minus u(850hPa)) (shaded) and relative humidity at 700hPa (contoured). Sold contour lines represent the positive relative humidity anomaly whereas the dashed contours represent the negative anomaly.

Figure 12. Distribution of SLP and SST anomalies from R8W for the combined impact of ENSO and NAO for two active TC years of 2005 (top panel) and 2010 (bottom panel). The different SST and SLP pattern likely causes different TC tracks and genesis locations for two active TC years of 2005 and 2010.

Figure 13. Left panel: Spatial anomaly distribution of z250 associated with ENSO (top), NAO (middle), and AMM (bottom) mode, respectively, captured from 20-member NR run data. Light green contours represent results from each member, and their average is contoured black. Variance in percentage averaged over 20 members is shown above each panel. Right panel: Temporal variation (PC time series) of each mode shown on the left panel. Temporal variations identified from each member are plotted by red-dashed lines, and black solid line with closed-circle represents their average. Time series in blue solid lines denote the Niño3.4 SST (top), NAO index (middle) and AMM index multiplied by 0.5 (bottom).

Figure 14. Signal-to-noise (S/N) ratio distributions of monthly variation of three leading modes (spatial distributions and their temporal variation) predicted by 20-member NR runs. The leading modes represented by SLP are shown on the left panel whereas the left panel the z250. S/N ratio lies in the range of 0 to 1. S/N ratio increases with decrease in intra-ensemble variance (i.e., residual variance).

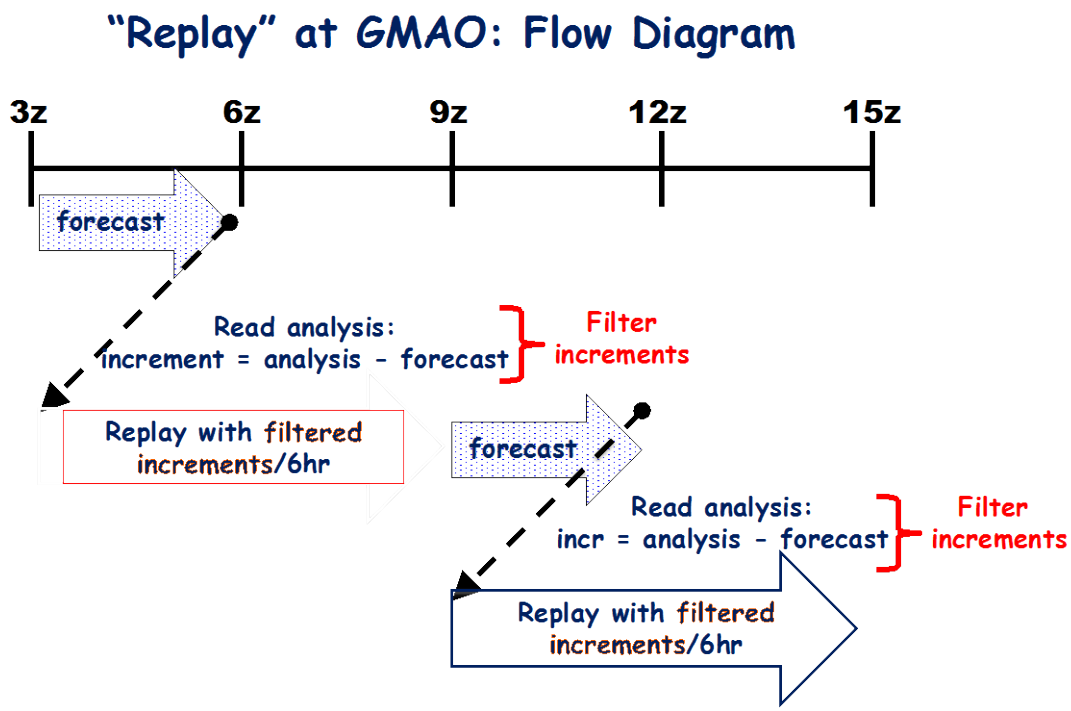

Figure 1. A schematic view of replaying the GEOS-5 model to an existing atmospheric analysis dataset. The process is generalized here to apply a filter to the full increments to allow constraining a subset of the flow.

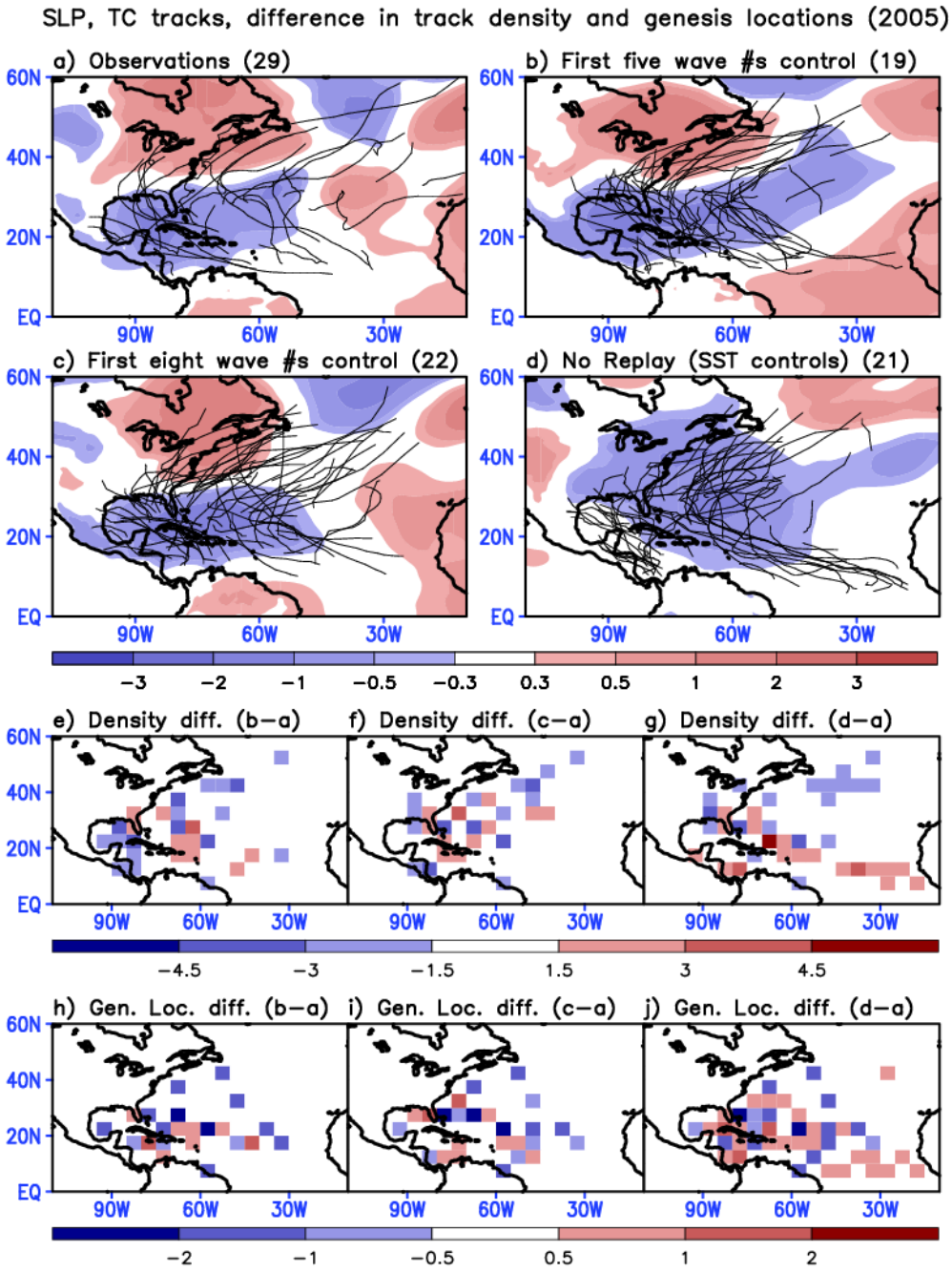

Figure 2. TC tracks for 2005 for a) observations, b) R5W, c) R8W and d) NR. All TC tracks produced by three member runs are plotted for R5W, R8W, and NR. Shading represents the three-member-averaged SLP anomaly for 2005. Number in parentheses above each panel is the average number of detected TCs across the three members. Panels of e, f, and g are distribution of differences in TC track density between model and observation (a). Bottom panels (h, i, and j) are distribution of differences in TC genesis locations between model and observation (a).

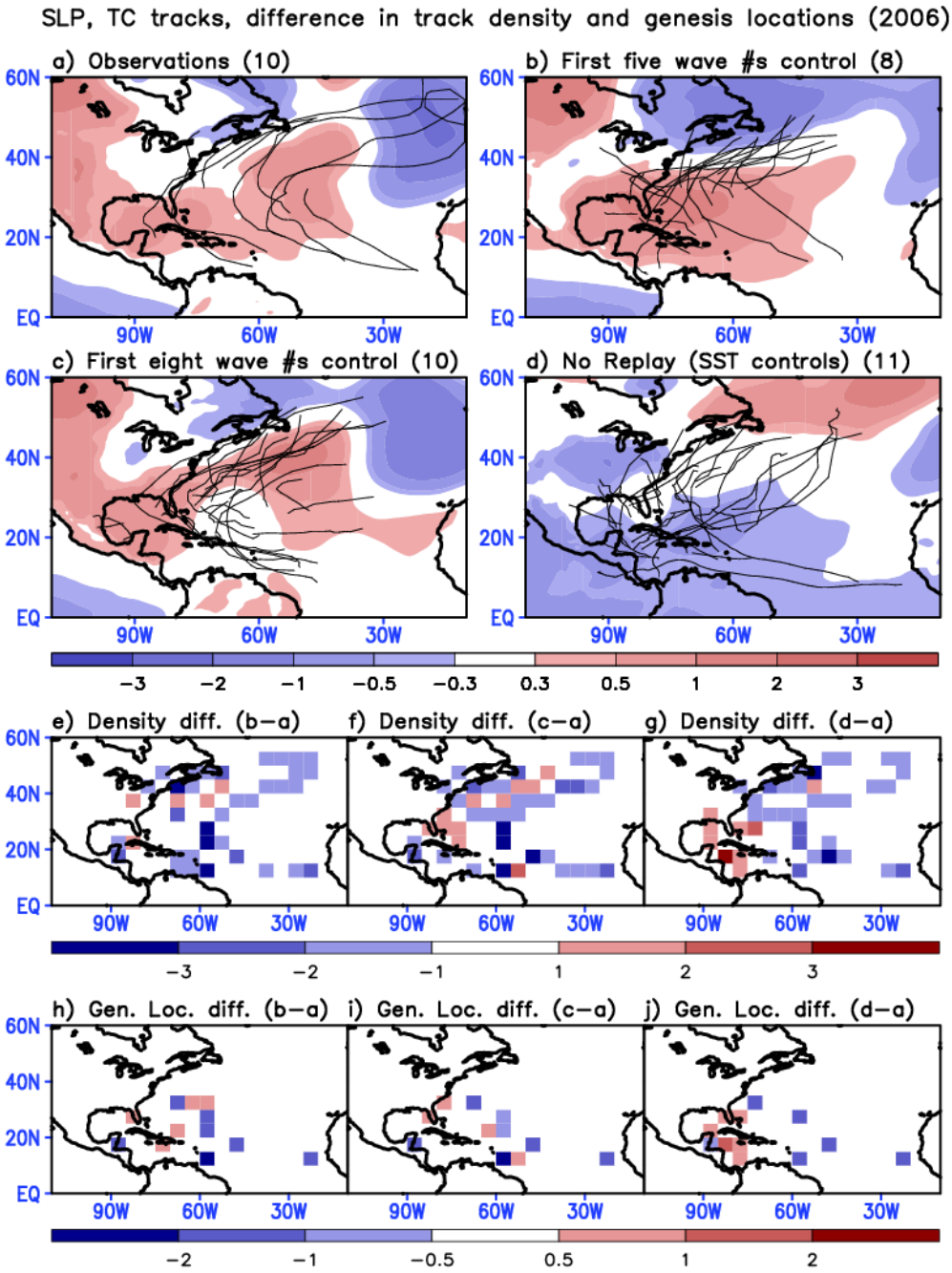

Figure 3. Same as Figure 2 but for 2006.

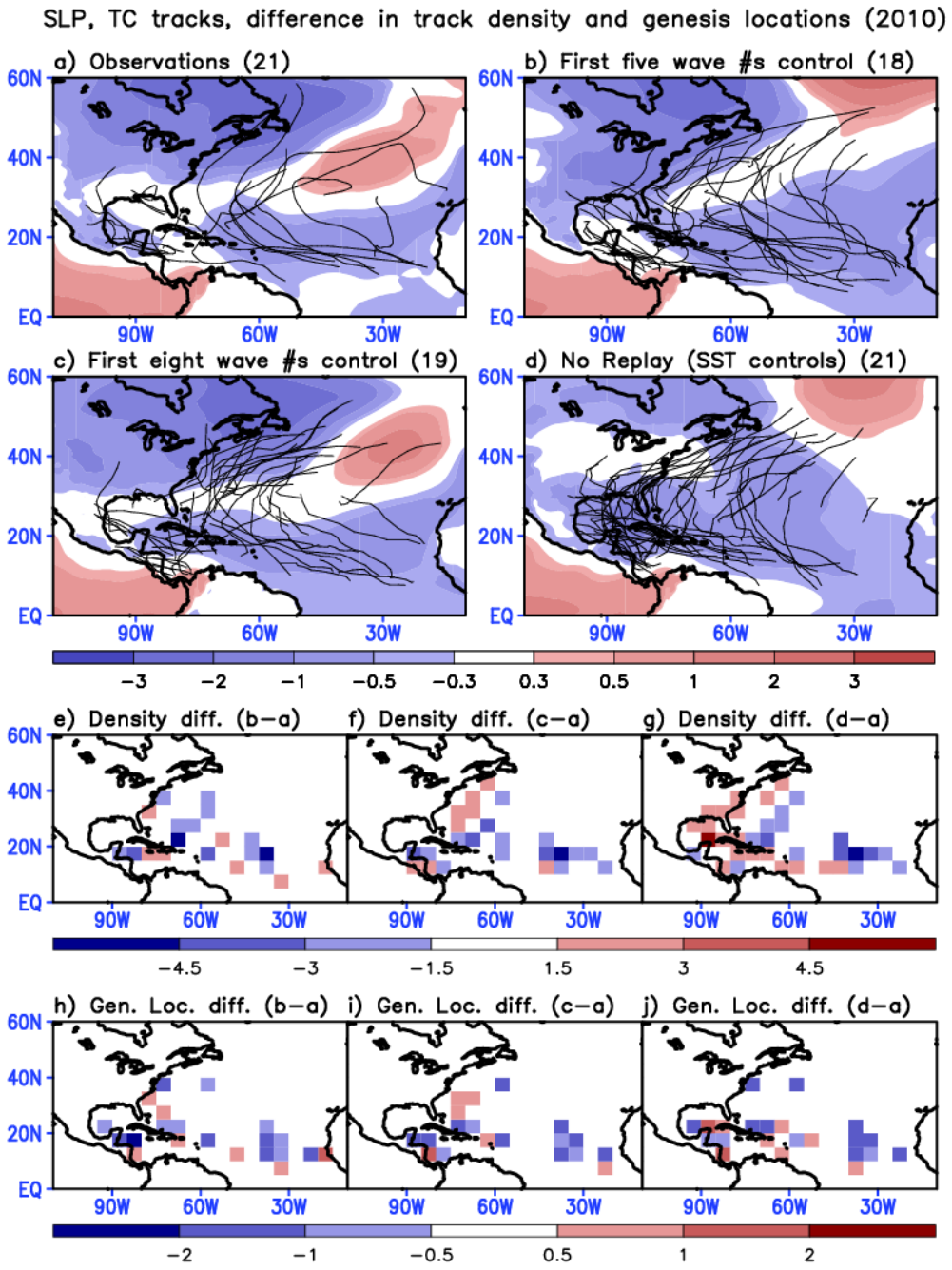

Figure 4. Same as Figure 2 but for 2010.

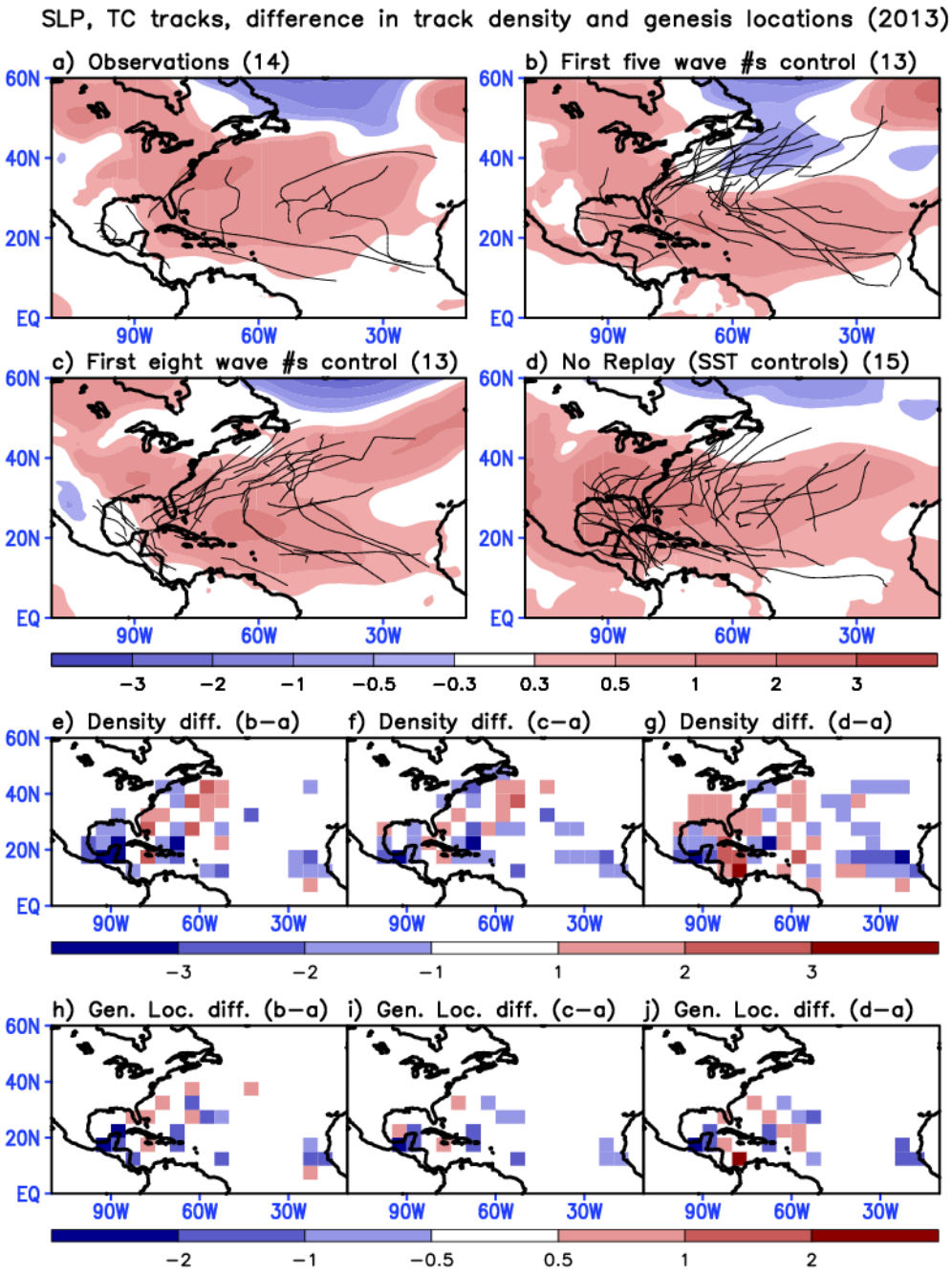

Figure 5. Same as Figure 2 but for 2013.

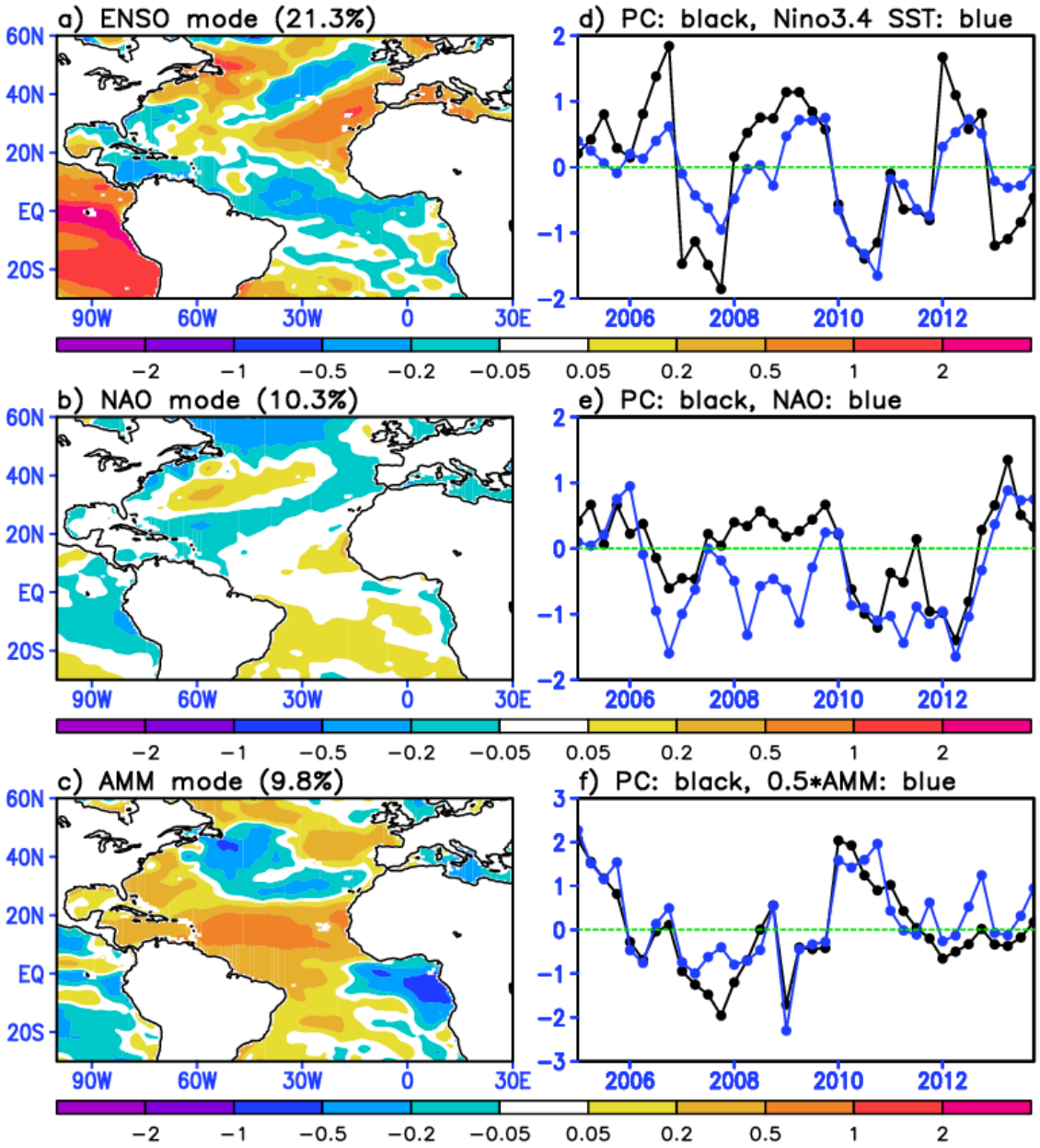

Figure 6. The first three rotated empirical orthogonal functions (REOFs) of the observed monthly SST for summer (June to September). The left panel represents the distribution of non-normalized eigenvectors whereas the right panel represents the corresponding PC time series (black solid line). Time series in blue solid lines denote, from the top to bottom panel, the Niño3.4 SST (top), NAO index (middle) and AMM index multiplied by 0.5 (bottom).

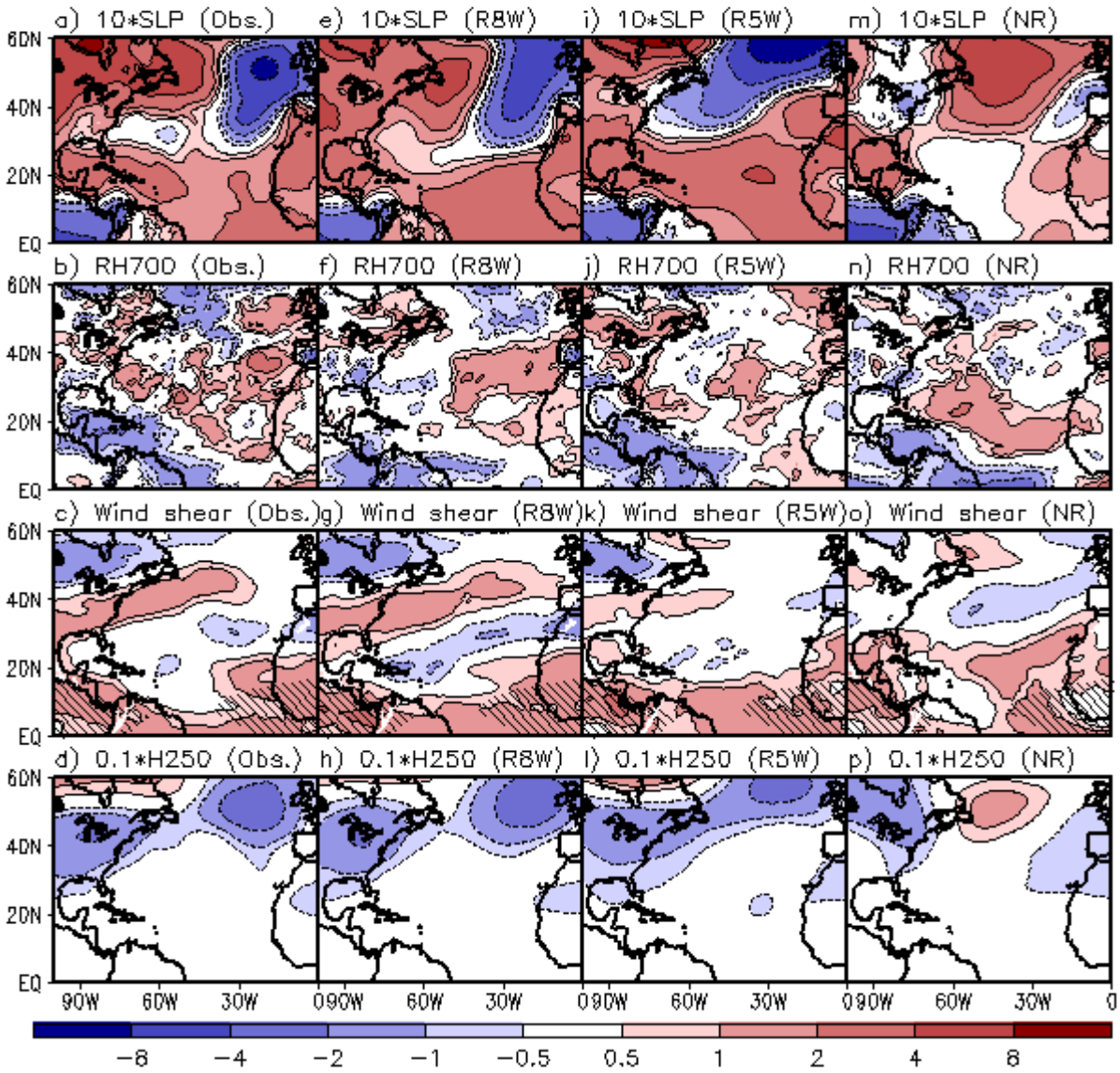

Figure 7. Anomaly distributions of the SLP (top row), relative humidity at 700hPa (second row), vertical wind shear (u(150hPa) minus u(850hPa)) (third row) and height at 250hPa (bottom row) regressed onto ENSO. Hatching in the third row panels represents climatologically the easterly wind shear region from observations. Each panel from the left represents the result for observation (first), R8W (second), R5W (third), and NR (fourth).

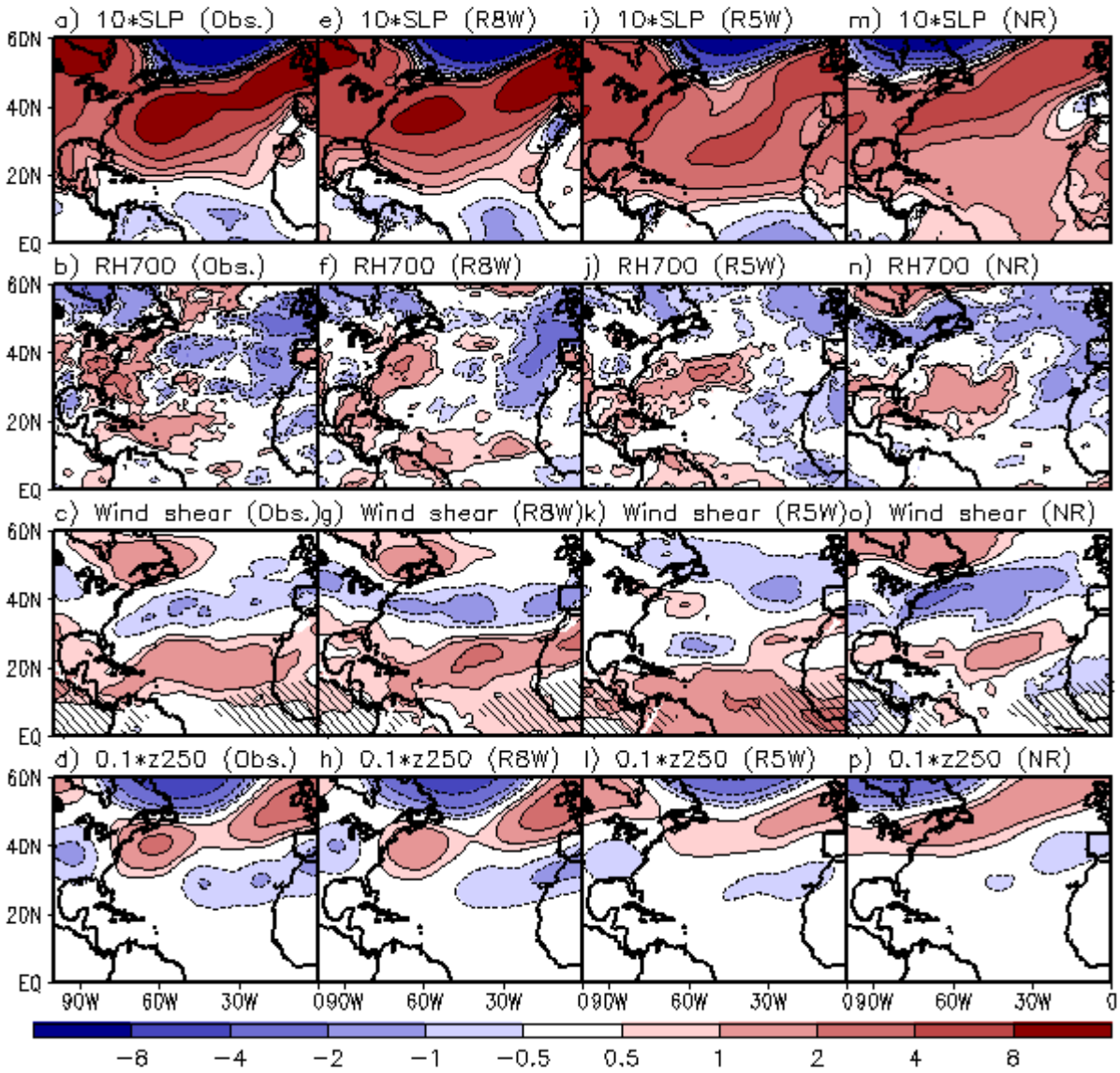

Figure 8. Same as Figure 7 but for the NAO.

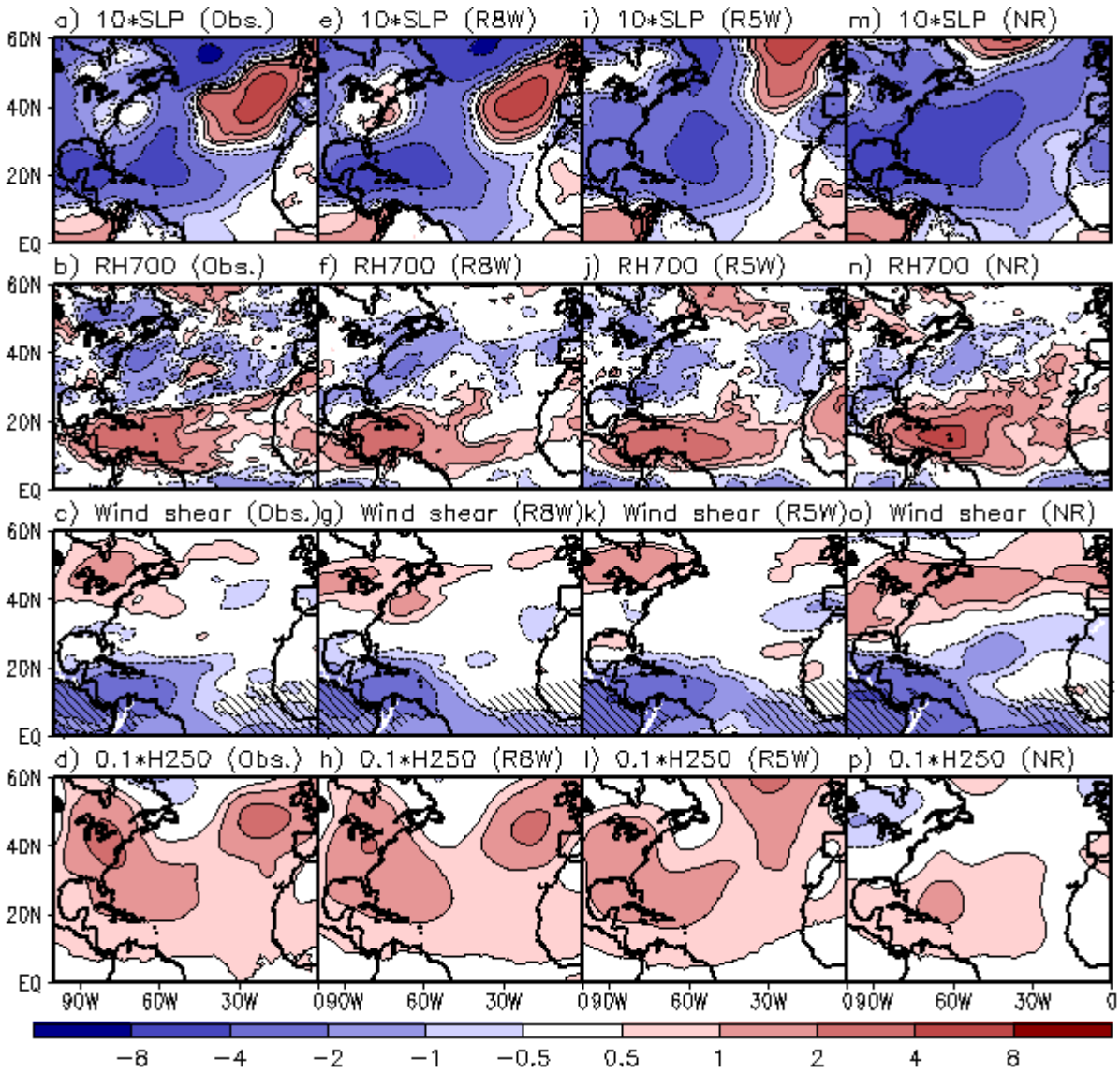

Figure 9. Same as Figure 7 but for the AMM.

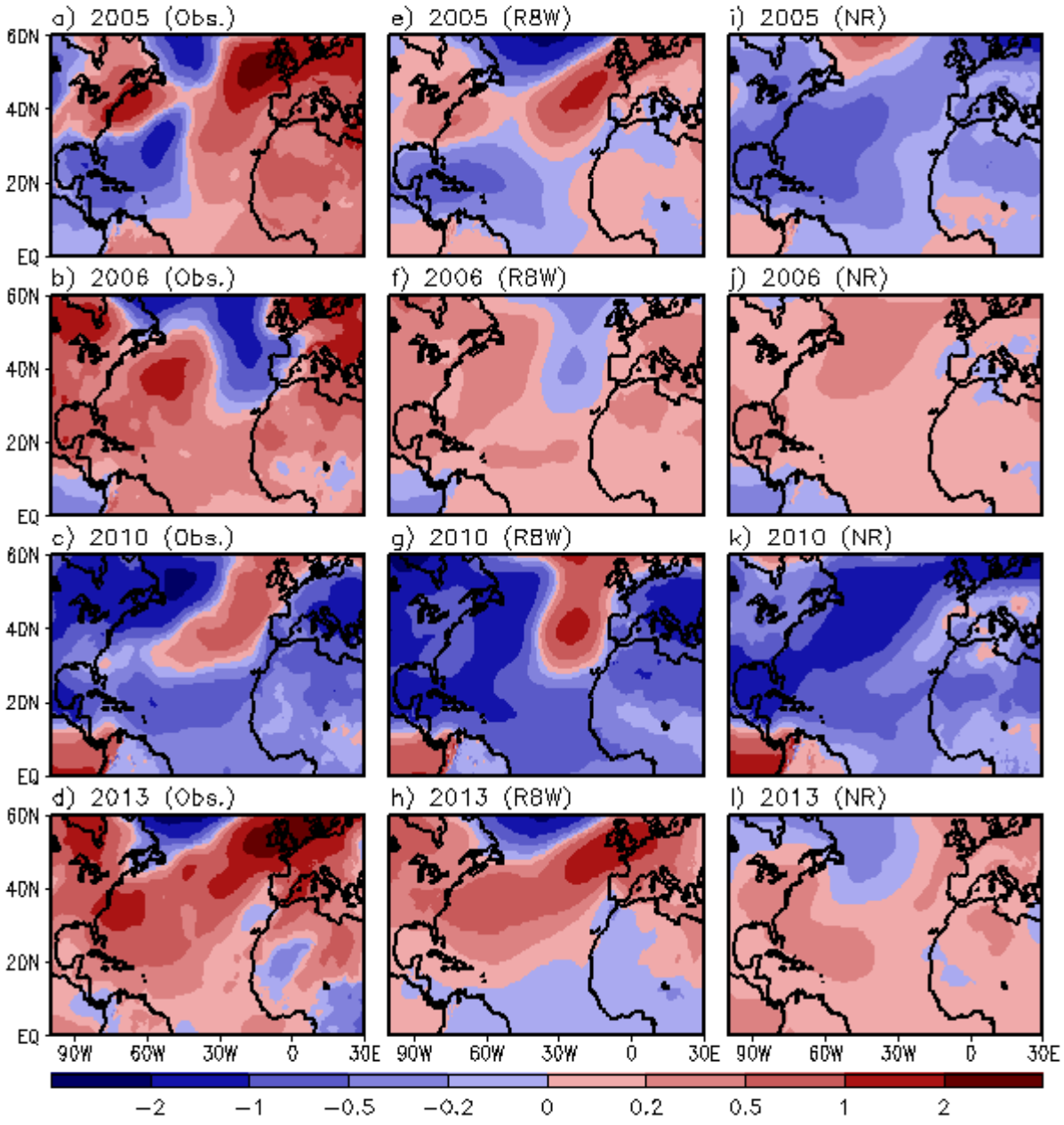

Figure 10. Distribution of SLP anomaly resulting from the combined effect of the ENSO, NAO and AMM. From the top to bottom panel, each panel represents the result for 2005, 2006, 2010 and 2013. Each panel from the left represents the result for observation (left), R8W (middle), and NR (right).

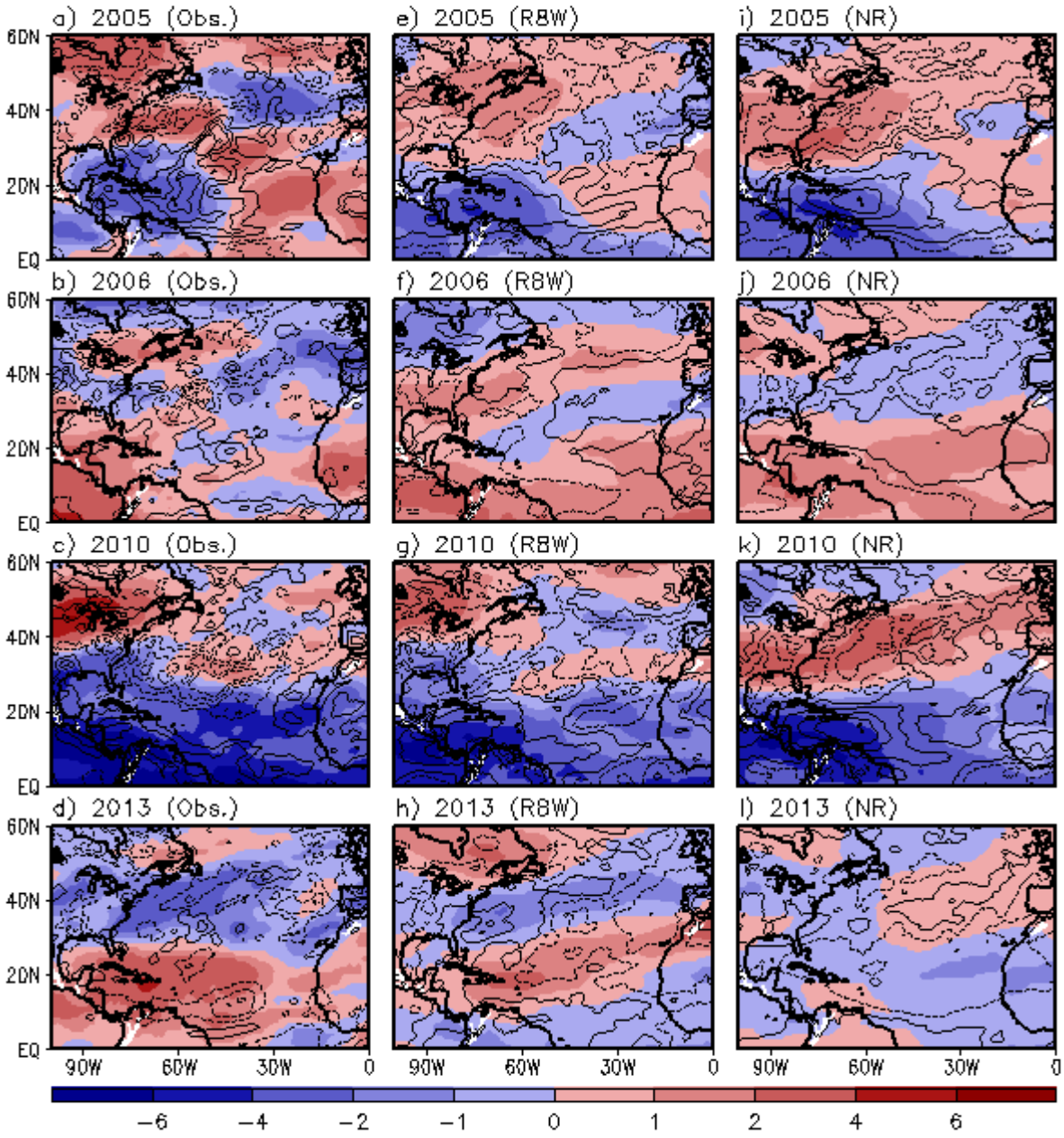

Figure 11. Same as Figure 10 but for vertical wind shear (u(150hPa) minus u(850hPa)) (shaded) and relative humidity at 700hPa (contoured). Sold contour lines represent the positive relative humidity anomaly whereas the dashed contours represent the negative anomaly.

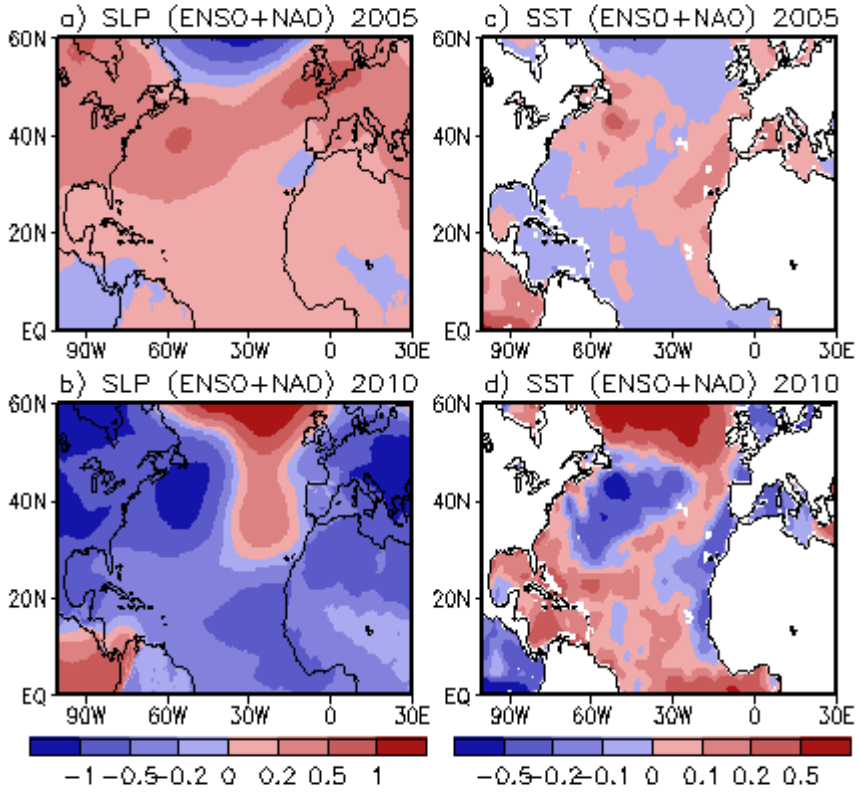

Figure 12. Distribution of SLP and SST anomalies from R8W for the combined impact of ENSO and NAO for two active TC years of 2005 (top panel) and 2010 (bottom panel). The different SST and SLP pattern likely causes different TC tracks and genesis locations for two active TC years of 2005 and 2010.

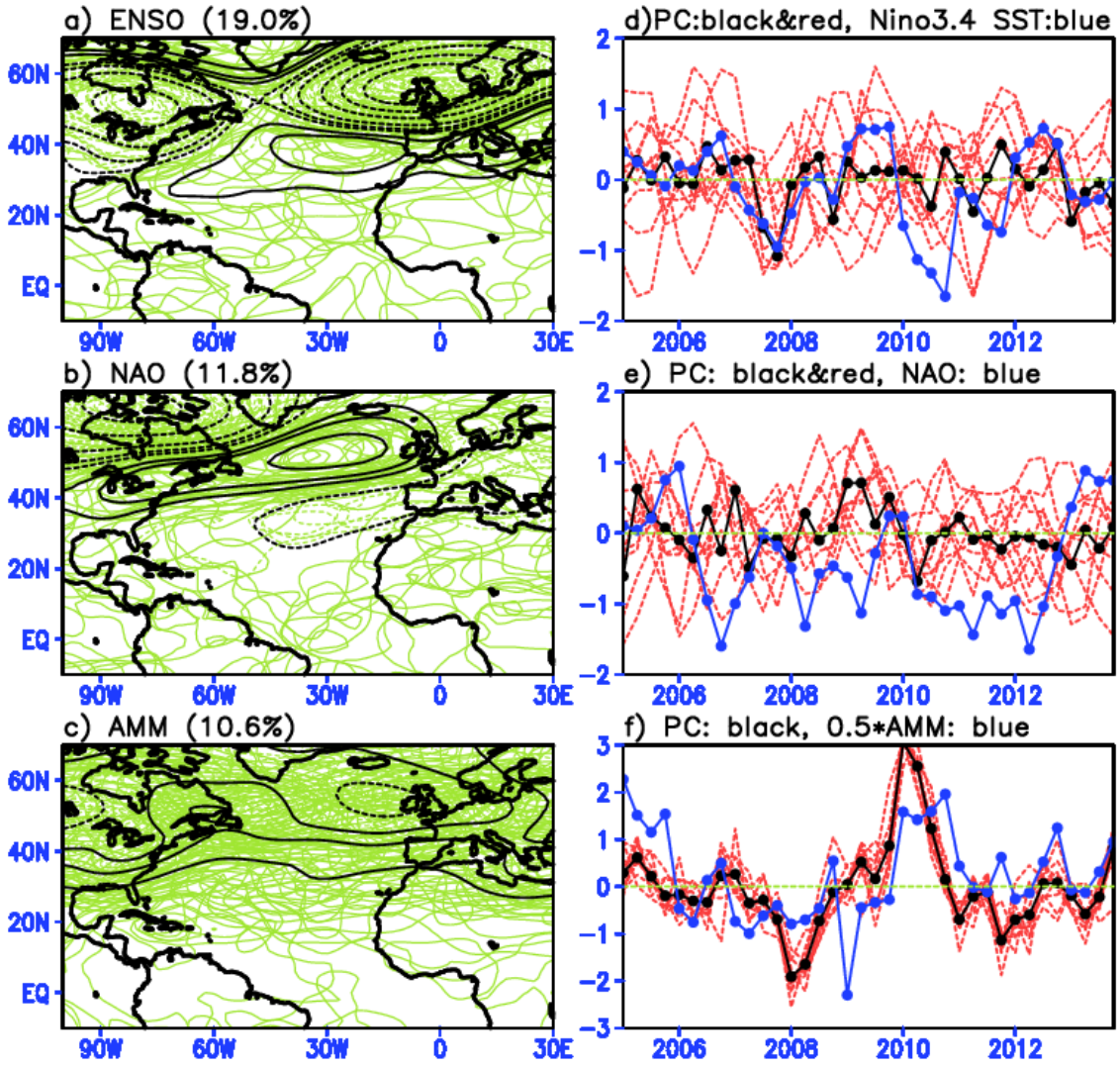

Figure 13. Left panel: Spatial anomaly distribution of z250 associated with ENSO (top), NAO (middle), and AMM (bottom) mode, respectively, captured from 20-member NR run data. Light green contours represent results from each member, and their average is contoured black. Variance in percentage averaged over 20 members is shown above each panel. Right panel: Temporal variation (PC time series) of each mode shown on the left panel. Temporal variations identified from each member are plotted by red-dashed lines, and black solid line with closed-circle represents their average. Time series in blue solid lines denote the Niño3.4 SST (top), NAO index (middle) and AMM index multiplied by 0.5 (bottom).

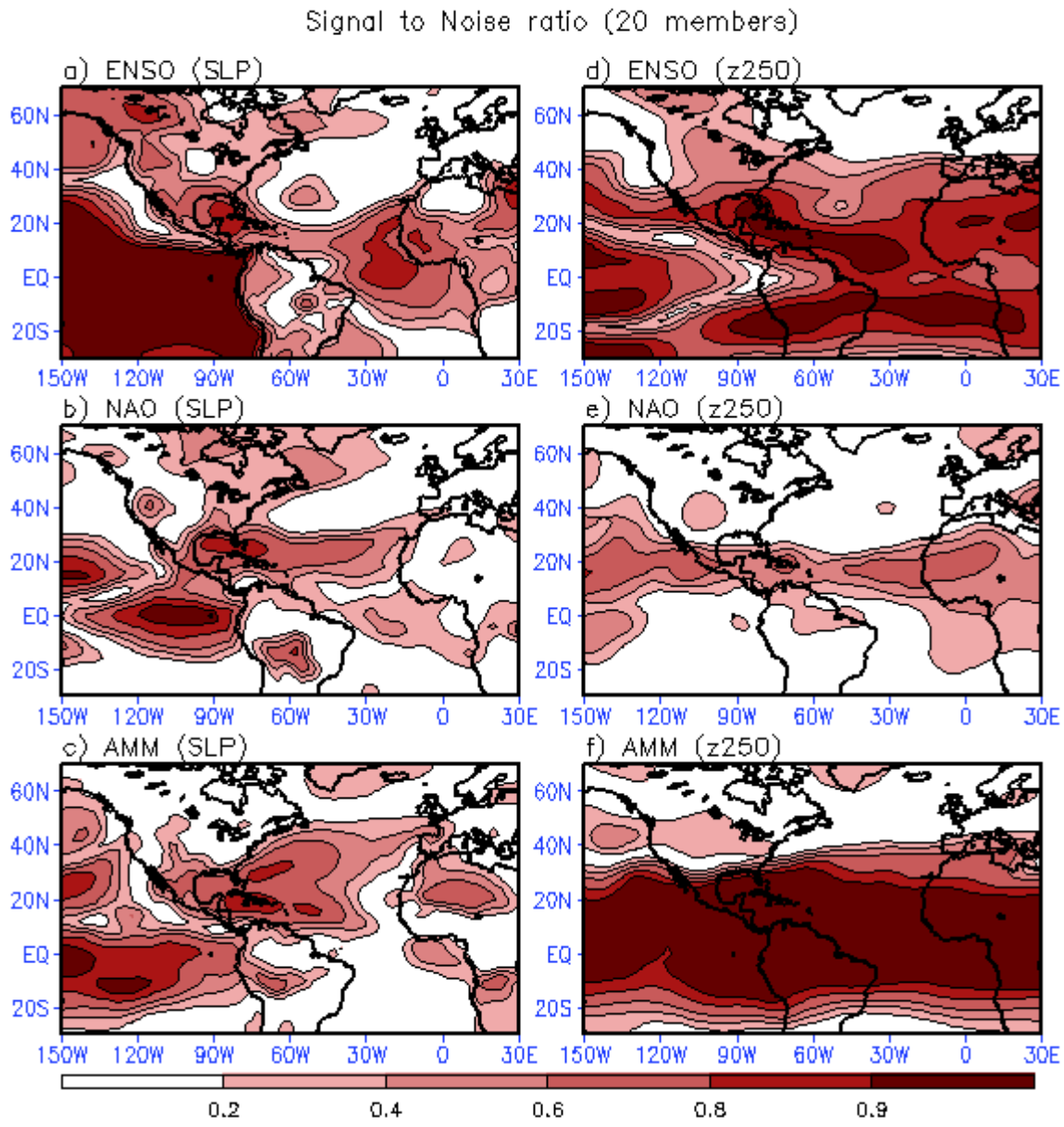

Figure 14. Signal-to-noise (S/N) ratio distributions of monthly variation of three leading modes (spatial distributions and their temporal variation) predicted by 20-member NR runs. The leading modes represented by SLP are shown on the left panel whereas the left panel the z250. S/N ratio lies in the range of 0 to 1. S/N ratio increases with decrease in intra-ensemble variance (i.e., residual variance).